

A GENUINELY MULTIDISCIPLINARY JOURNAL

CHEMPLUSCHEM

CENTERING ON CHEMISTRY

Accepted Article

Title: Catalysis and CO₂ capture by palladium incorporated covalent organic frameworks

Authors: Dhananjayan Kaleeswaran, Rajendran Antony, Abhishek Sharma, Ateeque Malani, and Ramaswamy Murugavel

This manuscript has been accepted after peer review and appears as an Accepted Article online prior to editing, proofing, and formal publication of the final Version of Record (VoR). This work is currently citable by using the Digital Object Identifier (DOI) given below. The VoR will be published online in Early View as soon as possible and may be different to this Accepted Article as a result of editing. Readers should obtain the VoR from the journal website shown below when it is published to ensure accuracy of information. The authors are responsible for the content of this Accepted Article.

To be cited as: *ChemPlusChem* 10.1002/cplu.201700342

Link to VoR: <http://dx.doi.org/10.1002/cplu.201700342>

WILEY-VCH

www.chempluschem.org

A Journal of



Catalysis and CO₂ capture by palladium incorporated covalent organic frameworks

Dhananjayan Kaleeswaran,^[a] Rajendran Antony,^[a] Abhishek Sharma,^[b,c,d] Ateeque Malani^[b] and Ramaswamy Murugavel*^[a]

^[a] Department of Chemistry, Indian Institute of Technology Bombay, Powai, Mumbai-400076, Maharashtra.

^[b] Department of Chemical Engineering, Indian Institute of Technology Bombay, Powai, Mumbai 400076, India.

^[c] IITB-Monash Research Academy, Indian Institute of Technology Bombay, Mumbai 400076, India.

^[d] Commonwealth Scientific and Industrial Research Organisation (CSIRO) Manufacturing, Clayton, Victoria 3169, Australia.

Abstract

Triazine based imine and β -ketoenamine linked COFs, TAT- DHBD (**1**) and TAT-TFP (**2**) have been synthesized from 1,3,5-tris-(4-aminophenyl)triazine (TAT) and 2,5-dihydroxybenzene-1,4-dicarboxaldehyde (DHBD) or 1,3,5-triformylphloroglucinol (TFP) under solvothermal conditions in dioxane/mesitylene mixture. These COFs exhibit significant surface area due to their meso- and micropores. The presence of basic nitrogen sites offers excellent affinity towards Pd nanoparticles and carbon dioxide. Post treatment of COFs **1** and **2** with palladium acetate gives Pd(II)/TAT-DHBD (**3**) and Pd(II)/TAT-TFP (**4**), which on reduction by NaBH₄ yields Pd(0)/TAT-DHBD (**5**) and Pd(0)/TAT-TFP (**6**), respectively. The new COFs have been characterized by FT-IR, solid-state ¹³C-NMR spectroscopy, XPS, SEM, TEM and BET surface area measurements. TEM studies corroborated uniform distribution of Pd(II) and Pd(0) sites in the COFs. **3-6** are active towards the Suzuki-Miyaura cross coupling of arenes with meager catalyst leaching even after five cycles. Besides, **4** exhibits CO₂ uptake of 11 wt % and 7.5 wt% at 273 and 298 K, respectively, at 1 bar.

Introduction

Covalent organic frameworks (COFs) are evolving as a special class of thermally stable crystalline porous polymers. Composed of light atoms such as B, C, N, O and H and linked *via* strong covalent bonds, enable them to function as low density materials.^[1] Judicious selection of organic building units and the reversible dynamic bond formation process paves way for fine tuning surface area, crystallinity, pore size and structural topology of these materials.^[1b,c,e,f,i] In the case of two-dimensional (2D) COFs, the organic building units integrate into a 2D-layered sheet which are stacked together with the help of π - π interactions and form periodic columnar π -arrangements with oriented one-dimensional (1D) channels ranging from a few angstroms to a few nanometers.^[2] The ordered π -arrangements and the accessible channels in the COFs offer opportunities for potential applications in the field of gas storage and separation,^[3] drug delivery,^[4] catalysis,^[5] energy storage and conversion,^[6] environmental remediation,^[7] membrane separation^[8] and proton conduction.^[9] Further, COFs decorated with fluorescent organic building units find applications in the area of sensing,^[10] optoelectronics,^[11] semiconductive and photoconductive devices.^[12]

The excellent stability and the availability of open cavities present in these COFs render them as outstanding supports for anchoring catalytically important metal nanoparticles.^{[5f],[13]} Further, the ordered and oriented 1D channels and inherent covalent bond design in the COFs make them better scaffolds than porous organic polymers (POPs) and metal organic frameworks (MOFs) for immobilizing the nanoparticles for efficient heterogeneous catalysis.^[14] Ultra-small metal nanoparticles can be introduced within the COF cavities through a confined synthesis approach.^{[5f-h],[13k],[15]} Remarkably, the COF scaffolds maintain framework integrity and crystallinity during the treatment with harsh reducing agents such as NaBH₄, LiAlH₄ or hydrazine to immobilize metal nanoparticles.^{[5i-k],[13k]} Among various transition metal nanoparticles loaded COFs that are explored as heterogeneous catalysts, palladium loaded COFs are particularly in high demand and are probed because of the tendency of Pd to make strong bonds with carbon.^[16,17]

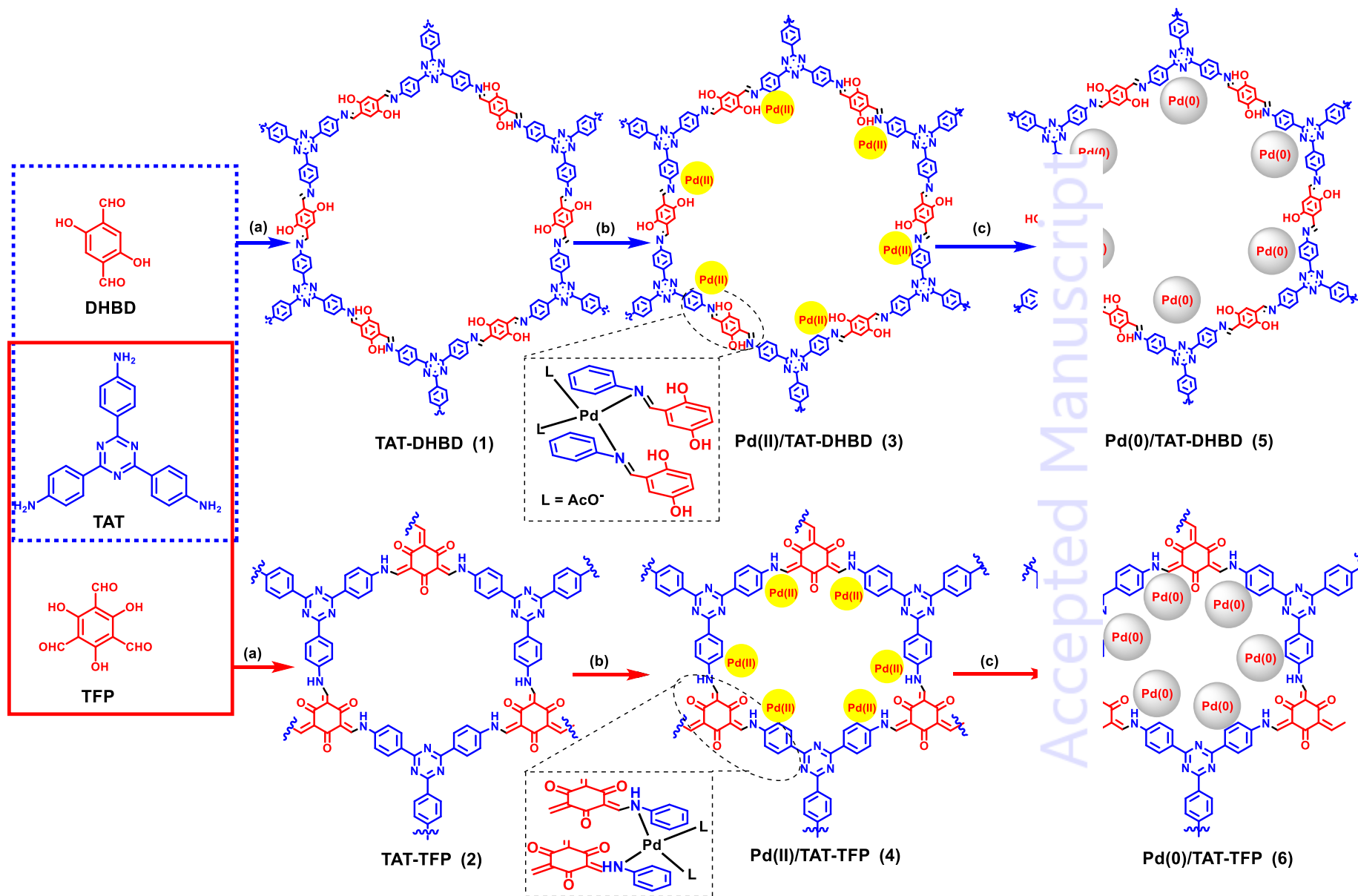
Imine linked COFs have served as excellent supports for the immobilization of metal nanoparticles. For example, Ding and others have demonstrated various C-C bond forming reactions and tandem reactions with Pd incorporated COFs.^{[5f-k],[13k]} One of the advantages of imine linked COFs is their stability towards water, acids and bases, apart from the strong interaction of Pd with imine nitrogen atom.^{[6c,e],[18]} Because of this interaction, there has been

a lot of interest to investigate N-rich COFs which contain a triazine core. Pd loaded N-rich COFs prevent leaching of Pd from the COF materials and increase the re-usability of catalyst without compromising on the conversion and product yield.^{[13k],[19]}

In addition to the catalysis, carbon dioxide capture and sequestration (CCS) is another important area of interest for both academicians and industrial communities.^{[20],[21]} Current technologies for CCS implement aqueous amine solutions such as monoethanolamine, methyldiethanolamine and piperazine as liquid adsorbents.^[22] The disadvantages of this method is the consumption of high energy during regeneration of trapped CO₂, as the CO₂ chemically interacts with amine solutions, apart from the toxicity, high volatility and corrosivity of the amine solutions.^[23] In order to overcome this, new alternatives have been suggested for CO₂ capture, e.g. various functionalized porous materials such zeolites,^[24] carbon-based sorbents,^[25] metal–organic frameworks (MOFs),^[26] covalent organic frameworks (COFs),^[3] mesoporous materials and porous organic frameworks (POFs).^[27] Among these materials, COFs have been extensively utilized for the CO₂ capture as they are highly stable (chemically and thermally). On the other hand, the building units of the COFs have been designed rationally with CO₂-philic nitrogen atoms. The ordered cavities can also be post modified with suitable functional groups to enhance the CO₂ capture.^[3d,g.] Recent work from our group has highlighted the importance of imine and aminal functional groups for CO₂ capture.^[10b] In the present investigation, we have examined imine and β -ketoenamine based triazine functionalized COFs TAT-DHBD (**1**) and TAT-TFP (**2**) as suitable scaffolds for incorporating Pd nanoparticles, and have further studied them as catalysts for C-C coupling reactions. We also demonstrate that these nitrogen rich COFs can be further used as CO₂ absorbing materials.

Results and Discussion

As shown in Scheme 1, the imine and β -ketoenamine linked COFs, namely TAT-DHBD (**1**) and TAT-TFP (**2**), were synthesized through condensing the amine (TAT) with respective aldehydes (DHBD and TFA) under solvothermal conditions using dioxane/mesitylene (1:1) mixture as solvent and aqueous acetic acid (6M) as catalyst in sealed glass tubes for three days at 120 °C. The COFs were washed with copious amount of acetone, THF and dichloromethane to ensure the complete removal of soluble impurities. Further, the COFs were soaked in acetone (2 days) followed by THF (2 days) for solvent exchange. During the course of the solvent exchange, the respective solvent was replaced after every 6 h. Subsequently each of the sample was heated at 120 °C under vacuum. The resultant COFs were



Scheme 1. Synthesis of TAT-DHBD (**1**), TAT-TFP (**2**) and their Pd embedded COFs; Conditions: (a) dioxane/mesitylene, 6M AcOH, 120 °C, 3 days; (b) Pd(OAc)₂, CH₂Cl₂, 24 h, RT; (c) NaBH₄, MeOH, 48 h, RT.

characterized by elemental analysis, FT-IR and cross polarization magic angle spinning (CP-MAS) ^{13}C NMR spectroscopy, thermal gravimetric analysis, powder X-ray diffraction and N_2 and CO_2 adsorption measurements.

The formation of new bonds and the structural integrity of the COFs have been investigated by FT-IR spectroscopy. TAT-DHBD (**1**) shows characteristic absorptions for azomethine ($\text{C}=\text{N}$) linkage at 1623 cm^{-1} and hydroxyl ($-\text{OH}$) stretching at 3352 cm^{-1} , whereas TAT-TFP (**2**) exhibits two bands at 1620 and 1572 cm^{-1} corresponding to carbonyl ($\text{C}=\text{O}$) and $-\text{C}=\text{C}-$ stretching vibrations arising out of keto-enol tautomerism between the hydroxyl group of phloroglucinol and the azomethine group.^{[18],[6c,e]} In addition, both the COFs exhibit C-N stretching vibration at 1293 and 1294 cm^{-1} , the aromatic $\text{C}=\text{C}$ stretching at 1432 and 1455 cm^{-1} and the aromatic C-H stretching bands around 3050 cm^{-1} , respectively. The stretching frequencies of COFs have been compared, in Figure 1, with the model Schiff base, TAT-Sal (**7**), which also exhibits similar vibrations. Besides, the attenuated bands around $3400\text{--}3300$ and 1700 cm^{-1} are attributed to terminal amine and aldehyde groups.^[28]

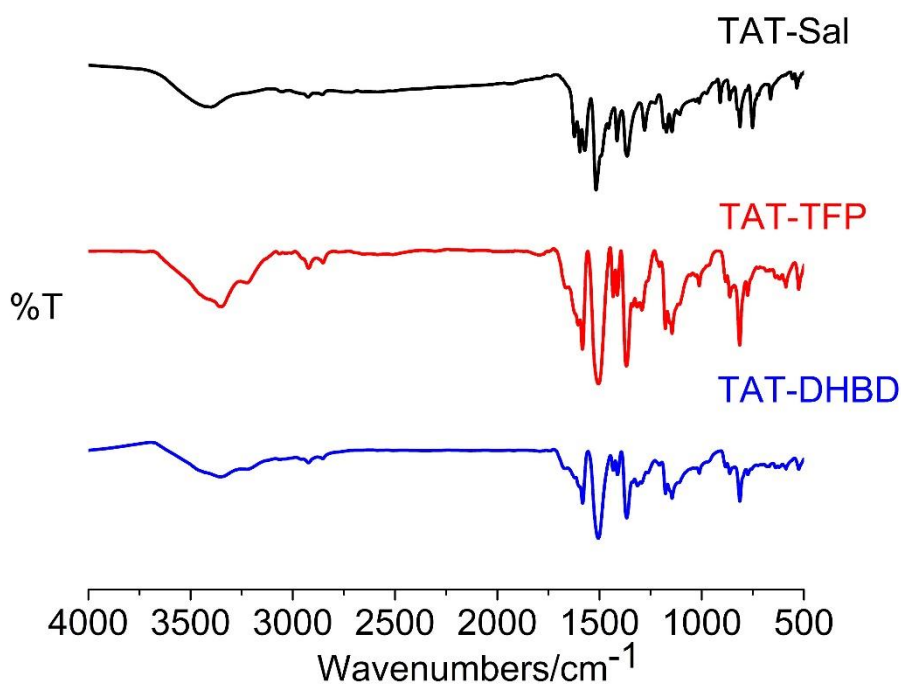


Figure 1. FT-IR spectra of TAT-Sal (**7**) (see ESI), TAT-TFP (**2**) and TAT-DHBD (**3**).

To further confirm the formation of imine and β -ketoenamine linkages, and the integrity of framework structure, CP-MAS ^{13}C NMR spectra of the solid samples have been investigated (Figure 2). The azomethine ($\text{C}=\text{N}$) carbon atoms in **1** resonate at 145 ppm while the aminal ($\text{CH}-\text{NH}$) carbons in **2** appear at 150 ppm . The resonance at 158 ppm is attributed to the carbon

atom attached to the hydroxyl group in TAT-DHBD (**1**) whereas the peak at 183 ppm corresponds to the carbonyl carbon atom of the TAT-TFP (**2**) due to keto-enol tautomerism.^[18] Both the COFs exhibit a resonance at 167 ppm corresponding to the carbon atom of the triazine core. The peaks in the range between 137 and 105 ppm are attributed to aromatic carbon atoms of the COFs (Figure 2).

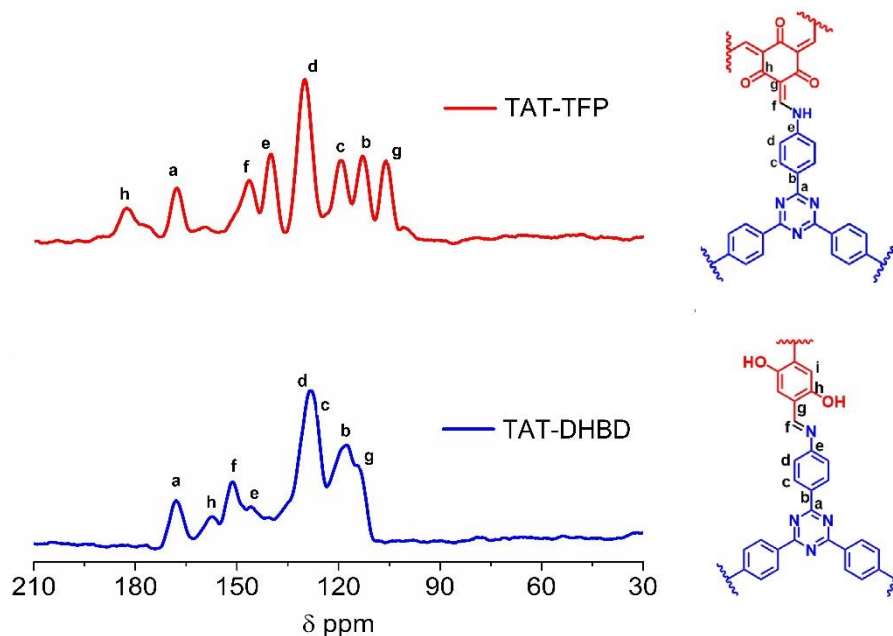


Figure 2. CP-MAS ^{13}C NMR spectra of TAT-DHBD (**1**) and TAT-TFP (**2**).

Thermogravimetric analysis of the new COFs were investigated by heating the activated samples under continuous flow of nitrogen at the heating rate of 10 °C/minute (Figure S3, SI). TAT-DHBD (**1**) is found to be stable up to 250 °C whereas TAT-TFP (**2**) exhibits an extended stability up to 400 °C. To confirm the hydrolytic and chemical stability, the COFs are dispersed in water, acid (1M) and base (9M) for seven days and characterized by the IR spectroscopy. The IR spectra of COFs exhibit similar spectral features of as-synthesized COFs, confirming that the structural integrity of the COFs is maintained even after soaking them in water, acid or base (Figure S4-S5, SI). The crystallinity of the pristine COFs were examined by PXRD measurements after treating them with water, HCl and NaOH (Figure S6, SI). While both COFs have been found to be perfectly stable in water. Further, while COF **2** exhibits no loss, a partial loss of crystallinity was observed for COF **1** when treated with HCl or NaOH.

The crystalline nature of the COFs were investigated by PXRD studies. The PXRD pattern reveals that the as synthesised COFs are highly crystalline with periodic hexagonal pores (Figure 3a and 3d). TAT-DHBD (**1**) exhibits peaks at $2\theta = 2.8, 4.9, 5.6, 7.4, 9.8$ and

26.3° corresponding to 100, 110, 200, 120, 220 and 001 planes, respectively. TAT-TFP (**2**) similarly exhibits peaks at $2\theta = 5.8, 10.0, 15.1$ and 26.5° for the 100, 110, 210 and 001 planes, respectively.^[29] The π - π interaction between the two sheets are derived from the d spacing of the 001 plane (26.5°) and it is calculated to be ~ 3.4 Å for both the COFs.

In order to glean more information from the above experimental PXRD results and determine the type of stacking, molecular dynamics (MD) simulations were performed to obtain relaxed configuration of both the COFs using the *Forcite* module of Materials Studio (see SI).^[30] We used various configurations obtained during the last 1 ns of the MD simulation and calculated the theoretical XRD patterns of the COFs using the *Reflex* module, resulting in good agreement with the experimental PXRD patterns (Figure 3). The combined PXRD and MD analysis establish slipped arrangement of both the COFs with stacking fault (Figure 3b, c and 3e, f), as COFs are energetically stable in slipped configurations.^[31]

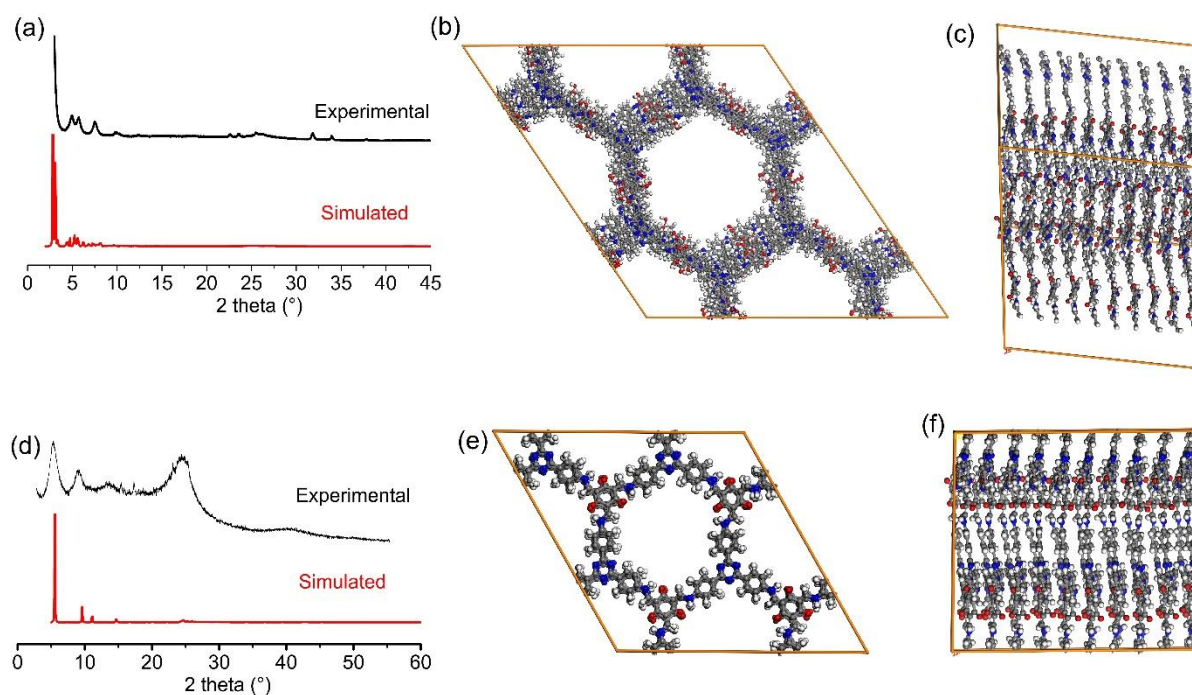


Figure 3. Comparison of the experimental and simulated PXRD pattern of (a) TAT-DHBD (**1**) and (d) TAT-TFP (**2**). Packing diagrams (b) and (c) show two perpendicular views of a minor slipped stacking of COF layers in **1**. Similarly (e) and (f) exhibit the slipped arrangement of **2** in perpendicular directions.

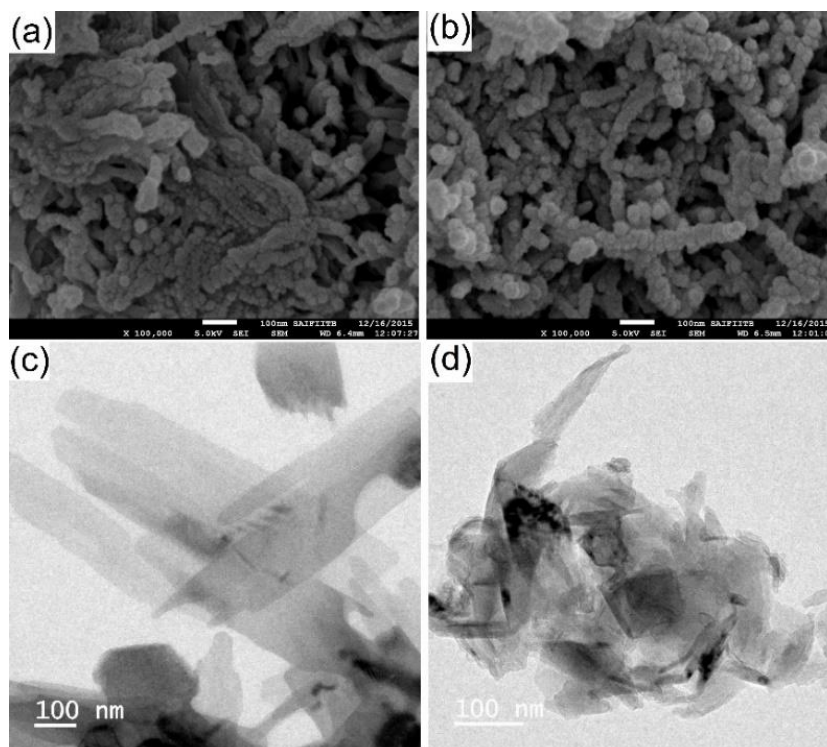


Figure 4. SEM images of (a) TAT-DHBD (**1**) and (b) TAT-TFP (**2**) and TEM images of (c) TAT-DHBD (**1**) and (d) TAT-TFP (**2**).

The morphology of the as-synthesized COFs were probed by field emission gun-scanning electron microscopy (FEG-SEM). Both the COFs exhibit similar morphology, where smaller spherical particles are connected to each other to form several hundred nanometer sized noodle like structures (Figure 4a and 4b). Transmission electron microscopy images of both the COFs exhibit layered structure which further confirms the formation of 2D- sheets with π - π stacking (Figure 4c and 4d).

The permanent porosity and pore size distribution of the COFs have been investigated by measuring N_2 adsorption isotherms at 77 K (Figure 5a). The nitrogen isotherm of TAT-TFP (**2**) exhibits classical Type I isotherm with increased nitrogen uptake at low partial pressures ($P/P_0 = 0.0$ to 0.1 bar), indicating the presence of permanent microporosity with reversible adsorption-desorption processes. On the other hand, the N_2 adsorption isotherm of TAT-DHBD (**1**) exhibits typical Type IV isotherm indicating the presence of mesopores in the later. In addition, the isotherm exhibits a hysteresis in the low pressure region ($P/P_0 < 0.30$), suggesting a swelling effect under liquid nitrogen temperature^[32] and significant interaction between the COF and the nitrogen gas. At higher pressures ($P/P_0 > 0.10$), nitrogen uptake increases due to capillary condensation.^[1a] The Brunauer–Emmett–Teller (BET) surface areas of TAT-DHBD

(1) and TAT-TFP (2) were estimated to be $750 \text{ m}^2\text{g}^{-1}$ and $646 \text{ m}^2\text{g}^{-1}$. The surface area of these COFs are high and are comparable to other reported structurally similar COFs (CCOF-1, $266 \text{ m}^2\text{g}^{-1}$ and CCOF-2, $335 \text{ m}^2\text{g}^{-1}$;[5e] COF-LZU1, $410 \text{ m}^2\text{g}^{-1}$;[5f] 2,3-DmaTph, $668 \text{ m}^2\text{g}^{-1}$;[5g] TpPa-1, $484 \text{ m}^2\text{g}^{-1}$;[5i] trzn-COF, $408 \text{ m}^2\text{g}^{-1}$;[13k] TRIPTA, $609 \text{ m}^2\text{g}^{-1}$;[29]). The pore size distribution (PSD) of the COFs has been evaluated from Non-Local Density Functional Theory (NLDFT) by fitting to the adsorption branch of nitrogen isotherm. The PSD study reveals the pore diameter of TAT-TFP (2) to be 11.7 \AA whereas TAT-DHBD (1) exhibits two pore diameters of 26.1 and 37.9 \AA , consistent with the Type I and IV isotherms exhibited by these two COFs, respectively (Figure 5b). The pore diameters obtained from the NLDFT method compare well with the values of 11.8 and 25.6 \AA obtained for COFs 2 and 1 from MD simulated structures. The other pore diameter of 37.9 \AA obtained from NLDFT presumably arises due to swelling effect at 77 K , which is seen from the hysteresis at low pressure region. The pore volumes of TAT-TFP (2) and TAT-DHBD (1) were calculated to be (from the nitrogen gas adsorbed at $P/P_0 = 0.99$) 0.36 and 0.44 cc g^{-1} , respectively. These results suggest that the pores in the TAT-TFP (2) and TAT-DHBD (1) would be accessible for hosting various gases such as CO_2 etc.

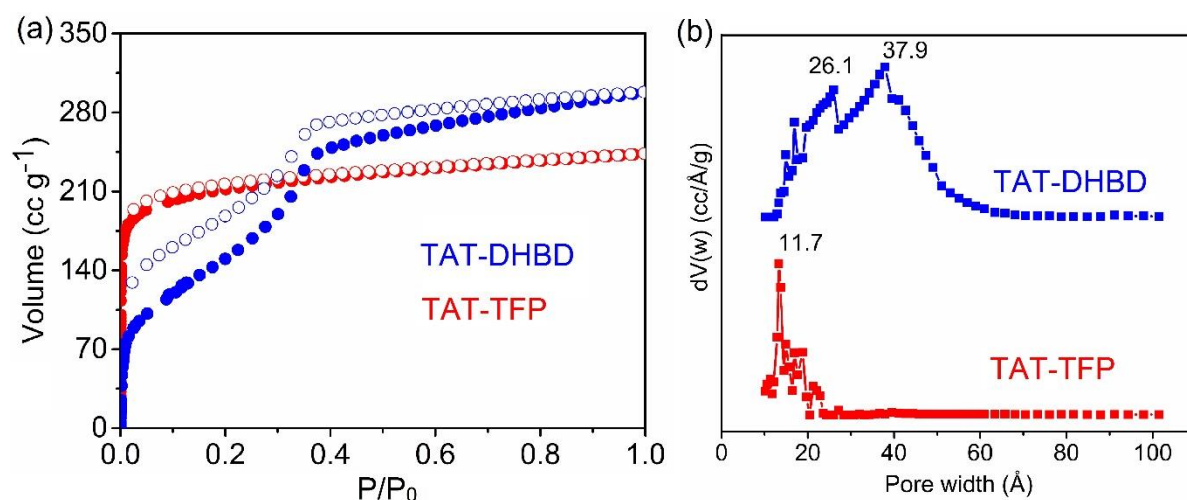


Figure 5. (a) Nitrogen sorption isotherm and (b) pore size distribution for TAT-DHBD (1) and TAT-TFP (2).

The high surface area, pore diameter, pore volume and the presence of nitrogen atoms in the form of imine and triazine functionalities prompted us to incorporate palladium metal ion or palladium nanoparticles in the COF materials and utilize the later in the catalysis. The Pd²⁺ incorporated COFs Pd(II)/TAT-DHBD (3) and Pd(II)/TAT-TFP (4) have been prepared by stirring TAT-DHBD (1) and TAT-TFP (2) with Pd(OAc)₂ at room temperature for 24 h.

The palladium nanoparticles embedded COFs Pd(0)/TAT-DHBD (**5**) and Pd(0)/TAT-TFP (**6**) have been synthesized by stirring a respective COFs in a methanolic solution of Pd(OAc)₂ followed by addition of excess amount of NaBH₄. The Pd loaded COFs have been characterized by elemental analysis, FT-IR, CPMAS ¹³C-NMR, TGA, PXRD, FE-SEM, EDAX analysis, HR-TEM and nitrogen sorption experiments.

FT-IR spectra of the pristine COFs **1** and **2** and Pd incorporated COFs **3-6** exhibit similar vibrational bands that correspond to the triazine core and imine functionalities (Figure 6), suggesting that the COF structures are preserved even after incorporation of Pd(II) or Pd(0) in their framework. The ¹³C CP/MAS NMR spectra of Pd(II)/TAT-DHBD (**3**), Pd(II)/TAT-TFP (**4**), Pd(0)/TAT-DHBD (**5**) and Pd(0)/TAT-TFP (**6**) (Figure 7) are almost identical to those of the pristine COFs **1-2** in the phenyl region, also confirming the preservation of pristine COF structures after the metal incorporation. In the case of Pd(II)/TAT-DHBD (**3**) and Pd(II)/TAT-TFP (**4**), two additional minor peaks appear at 179 and 23 ppm, corresponding to the carbonyl and methyl groups of the acetate ligand in Pd(OAc)₂. Free Pd(OAc)₂ exhibits carbonyl carbon resonance at 190 ppm.^[5f] Thus, the observed upfield shift of 11 ppm confirms the strong binding of Pd(OAc)₂ with COFs. Thermogravimetric analysis of Pd incorporated COFs exhibit gradual and continuous weight-loss above 140 °C under nitrogen atmosphere, similar to the thermal behaviour of other Pd loaded COFs described earlier (Figure S15, SI).^{[5f,i],[13k]}

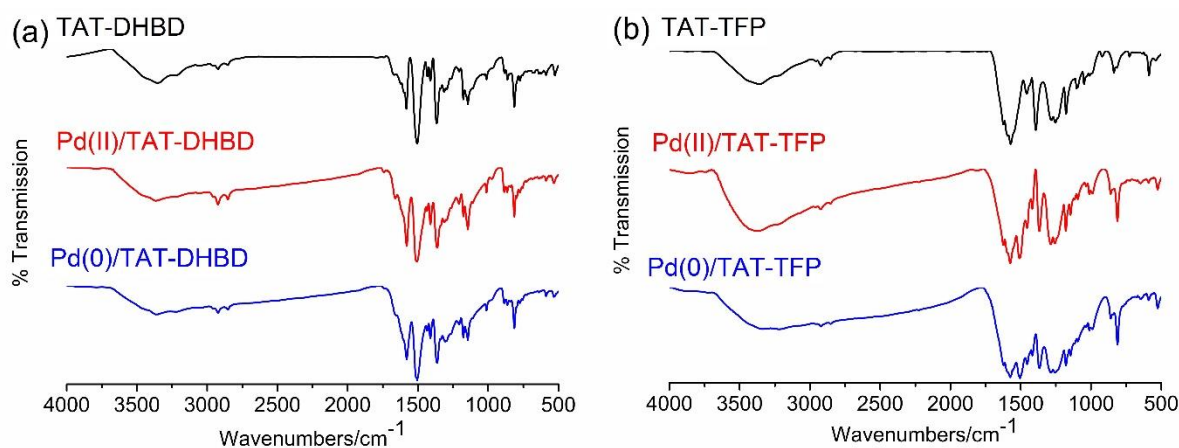


Figure 6. FT-IR spectra of a) TAT-DHBD (**1**), Pd(II)/TAT-DHBD (**3**) and Pd(0)/TAT-DHBD (**5**); b) TAT-TFP (**2**), Pd(II)/TAT-TFP (**4**) and Pd(0)/TAT-TFP (**6**).

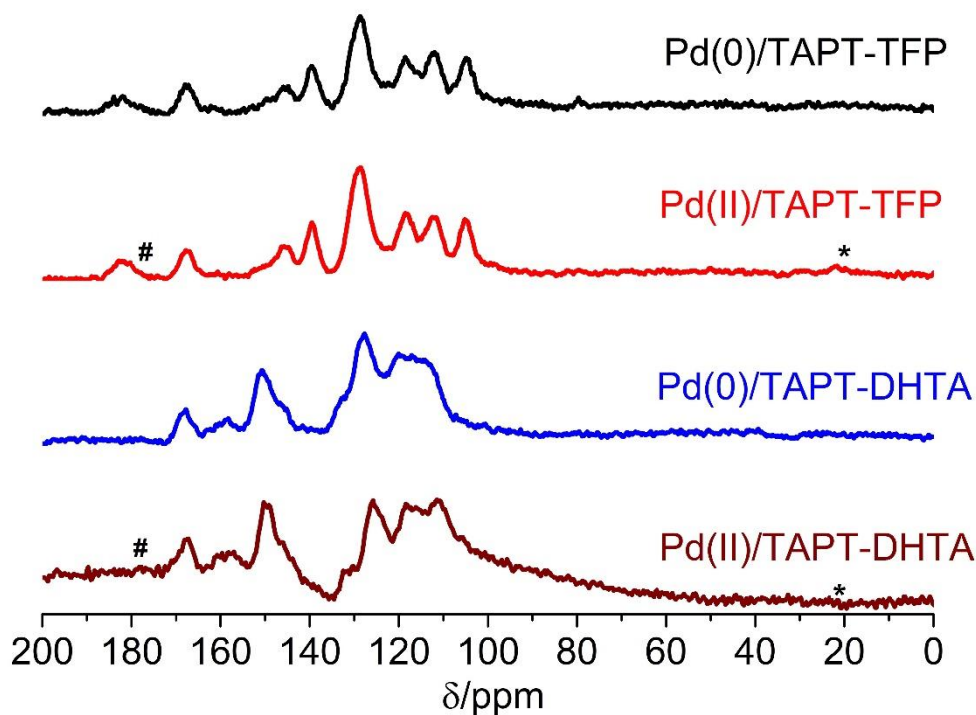


Figure 7. CP-MAS ^{13}C NMR spectra of Pd(II)/TAT-DHBD (**3**), Pd(II)/TAT-TFP (**4**), Pd(0)/TAT-DHBD (**5**) and Pd(0)/TAT-TFP (**6**) (* represents CH_3 resonances at 23 ppm and # represents $\text{C}=\text{O}$ resonance 179 ppm).

The observed PXRD pattern of each of the Pd loaded COFs is almost identical to the corresponding pristine COFs, suggesting only a minor loss of crystallinity of the COFs after Pd incorporation (Figures 3 and Figure S17, SI). In the case of Pd(0)/ TAT-DHBD (**5**) and Pd(0)/ TAT-TFP (**6**), additional peaks appear at $2\theta = 40^\circ$ and 47.5° , due to the presence of embedded metallic Pd nanoparticles in the COF structures.^[13k] Since Pd nanoparticles are incorporated between the interlayers of 2D sheets, it affects the π - π stacking, which is evident from the slight broadening of the (001 plane) peaks at $2\theta = 26.5^\circ$.^[5i]

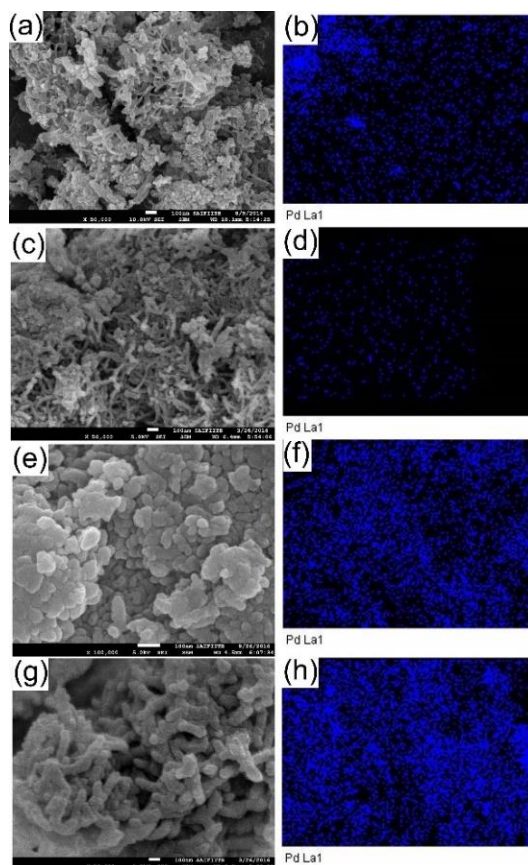


Figure 8. SEM images of Pd(II)/TAT-DHBD (3), Pd(II)/TAT-TFP (4), Pd(0)/TAT-DHBD (5) and Pd(0)/TAT-TFP (6) ((a), (c), (e), (g)) and their respective EDS for Pd ((b), (d), (f), (h))

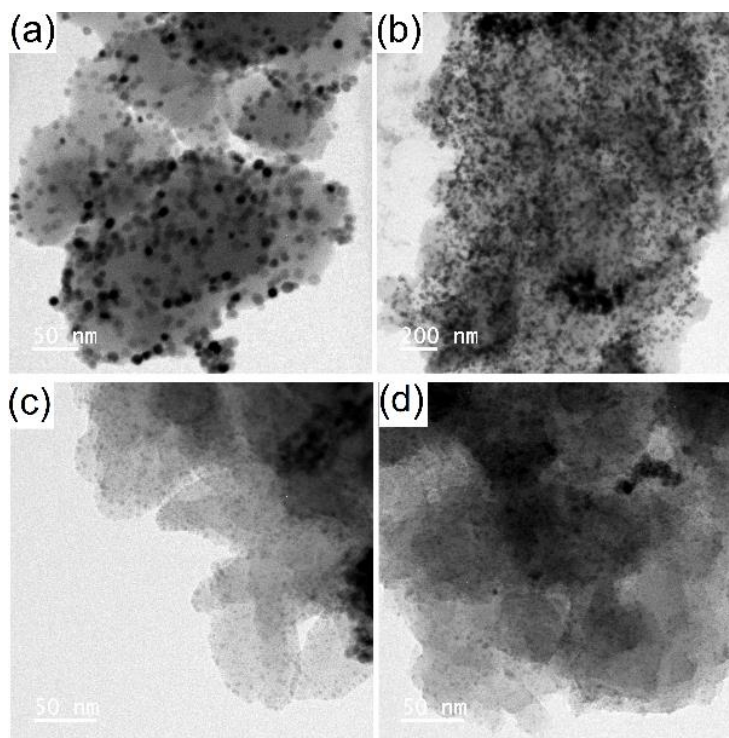


Figure 9. TEM images of (a) Pd(II)/TAT-DHBD (3), (b) Pd(II)/TAT-TFP (4), (c) Pd(0)/TAT-DHBD (5) and (d) Pd(0)/TAT-TFP (6).

FE-SEM analysis indicate that the morphology of the Pd incorporated COFs are also identical to those of the corresponding pristine COFs (Figure 8, left column), further suggesting the structural integrity of COFs even after treatment with Pd(OAc)₂. Energy dispersive X-ray analysis (EDX)-elemental mapping of Pd incorporated COFs shows that the Pd nanoparticles are homogeneously dispersed over the frameworks (Figure 8, right column). The Pd loadings in the COFs has also been evaluated from the EDX analysis.^[33] It is found that 10.5 and 14.9 wt % of Pd is loaded in Pd(II)/TAT-DHBD (**3**) and Pd(II)/TAT-TFP (**4**), while 11.4 and 10.6 wt % of Pd is loaded in the case of Pd(0)/TAT-DHBD (**5**) and Pd(0)/TAT-TFP (**6**). Similar results were found from the TGA traces of Pd incorporated COF under air (**3**, 7.5 wt %; **4**, 18.3 wt %; **5**, 15.7 wt % and **6**, 9.9 wt %) (Figure S16, SI). FEG-TEM studies reveal that the layered-structure of pristine COFs, which once again remained unchanged even after Pd nanoparticles incorporation. Besides, Pd(0) nanoparticles (< 5 nm) are uniformly dispersed in the pores of the COFs (Figure 9 and Figure S18, SI). The TEM analyses of Pd(II) incorporated COFs **3** and **4** exhibit aggregation of bigger nanoparticles. It appears that, due to high acceleration potential of 300 kV used for TEM studies, conversion of Pd(II) to Pd(0) takes place (Figure 9a and 9b). Similar reduction behaviour under TEM beam has been observed in other Pd-COFs earlier in the literature.^[5i]

To further investigate the incorporation of Pd nanoparticles into the COFs and as well as to establish the oxidation state of Pd species in the framework, X-ray photoelectron spectroscopy (XPS) measurements have been carried out. The binding energies obtained are presented in Table 1. Pd(II)/TAT-DHBD (**3**) and Pd(II)/TAT-TFP (**4**) exhibit characteristic peaks for Pd 3d_{5/2} at 337.9 and 337.86 eV, respectively, while the peaks for Pd 3d_{3/2} are observed at 343.2 and 343.1 eV, respectively (Figure 10a and 10c). This confirms the presence of Pd in +2 oxidation state. The observed binding energy values are negatively shifted by ~0.5 eV in comparison to free Pd(OAc)₂ (338.4 eV), suggesting strong bonding of Pd(OAc)₂ with the framework.^[5f,i] Pd(0)/TAT-DHBD (**5**) and Pd(0)/TAT-TFP (**6**) further exhibit characteristic peaks for Pd 3d_{5/2} at 335.5 and 335.8 eV, whereas the peaks for Pd 3d_{3/2} are observed at 340.7 and 341.1 eV, respectively, confirming that Pd is present in the zero oxidation state.^{[5i],[13k]} Besides, slender humps are observed at 337.0 and 343.1 eV due to the incomplete reduction of Pd(II) by NaBH₄ for both **5** and **6**.

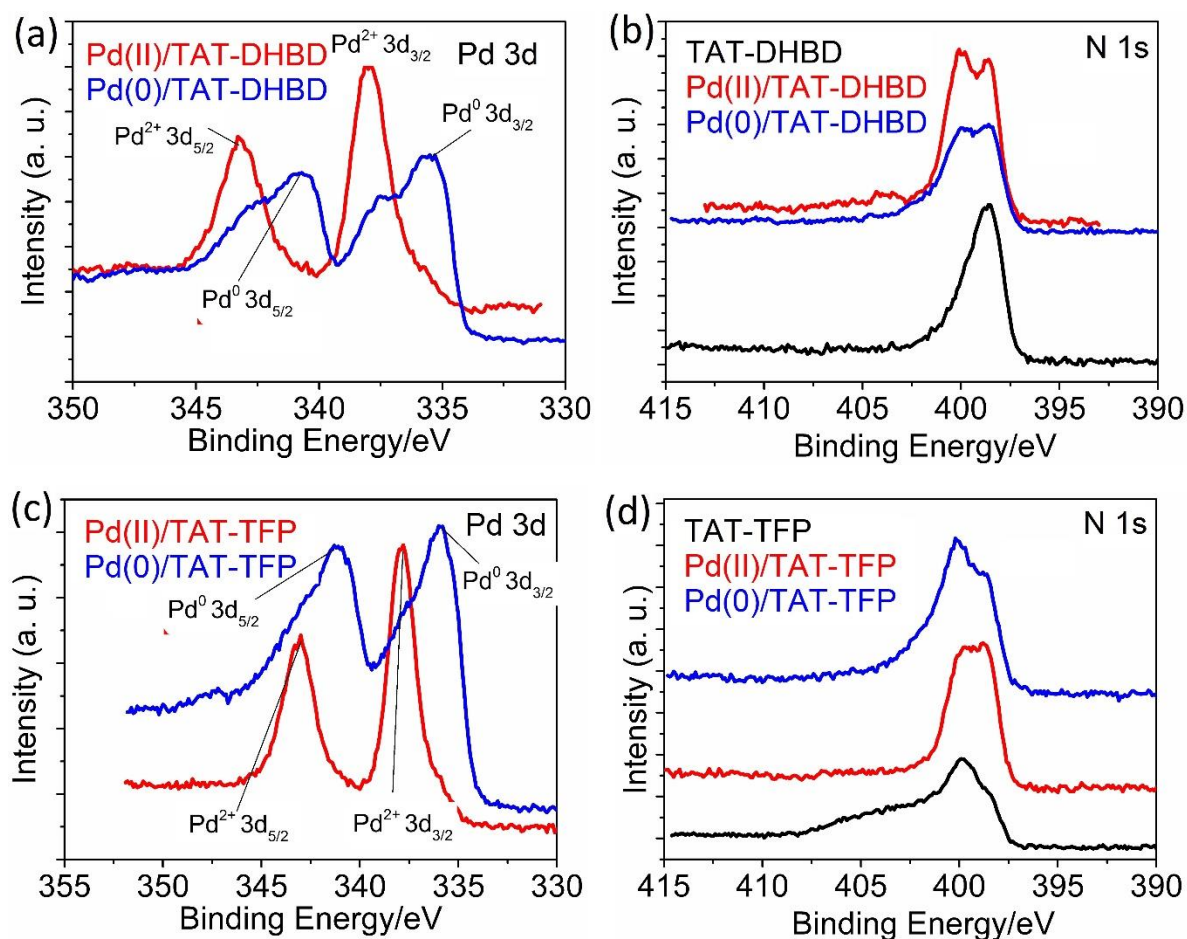


Figure 10. XPS spectra of (a) Pd(II)/TAT-DHBD (3) and Pd(0)/TAT-DHBD (5) in Pd 3d region; (b) TAT-DHBD (1), Pd(II)/TAT-DHBD (3) and Pd(0)/TAT-DHBD (5) in N 1s region; (c) Pd(II)/TAT-TFP (4) and Pd(0)/TAT-TFP (6) in Pd 3d region and (d) TAT-TFP (2), Pd(II)/TAT-TFP (4) and Pd(0)/TAT-TFP (6) in N 1s region.

Table 1. Binding energies of the Pd 3d_{3/2}, Pd 3d_{5/2}, N 1s and O 1s from the XPS

COFs/Elements	Pd 3d _{3/2}	Pd 3d _{5/2}	N 1s	O 1s
TAT-DHBD (1)	-	-	398.6	532.2
Pd(II)/TAT-DHBD (3)	343.2	337.9	398.6, 400.0	532.1
Pd(0)/TAT-DHBD (5)	340.7	335.5	398.6, 399.9	532.1
TAT-TFP (2)	-	-	398.5, 399.7	531.9
Pd(II)/TAT-TFP (4)	343.1	337.8	398.7, 400.1	531.9
Pd(0)/TAT-TFP (6)	341.1	335.8	398.7, 400.1	532.4

N 1s XPS spectrum of TAT-DHBD (**1**) exhibits only one peak at 398.6 eV, which is assigned to the triazine and imine nitrogen (both the nitrogen atoms are chemically equivalent (C=N)), while TAT-TFP (**2**) exhibits two peaks at 399.7 (aminal nitrogen) and 398.5 eV (triazine core). After the treatment of Pd(OAc)₂ the peaks for the N 1s in Pd(II)/TAT-DHBD (**3**) and Pd(II)/TAT-TFP (**4**) are shifted to 399.9 and 400.1 eV, respectively (Figure 10b and 10d). This observation confirms the coordination of imine and aminal nitrogen to Pd. The non-participation of phenolic group in coordination has been confirmed from the O 1s XPS spectra of TAT-DHBD (**1**), Pd(II)/TAT-DHBD (**3**) and Pd(0)/TAT-DHBD (**5**) since all the three COFs exhibit a peak at ~532.2 eV, with no observable shifts (Figure S20b and S21b, SI).

The permanent porosity and pore size distribution of the Pd incorporated COFs have been evaluated by nitrogen sorption measurements at 77 K and 1 bar (Figure 11). The BET surface area of the COFs has significantly reduced on metal loading, suggesting that the Pd nanoparticles are presumably embedded within the pores of the COFs (Table 2). Pore size distribution of the Pd loaded COFs have also been obtained from NLDFT calculations by fitting the adsorption branch of the nitrogen isotherm. From the above studies (such as SEM, TEM, XPS and surface area analysis), it is clear that Pd(II) and Pd(0) are finely dispersed inside the pore surface and also in between the layers of the COF matrix.

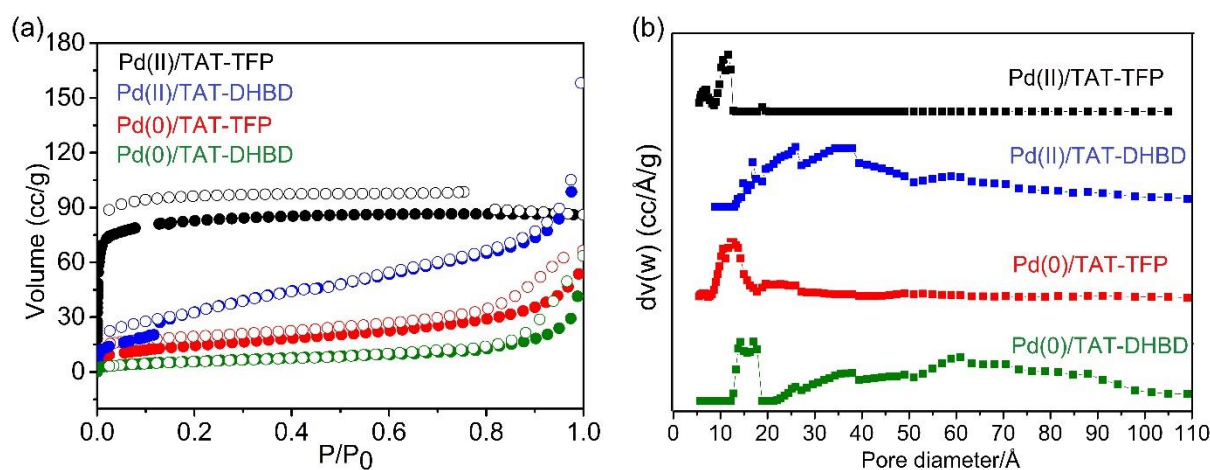


Figure 11. (a) Nitrogen sorption isotherms and (b) Pore size distribution of Pd(II)/TAT-DHBD (**3**), Pd(II)/TAT-TFP (**4**), Pd(0)/TAT-DHBD (**5**) and Pd(0)/TAT-TFP (**6**).

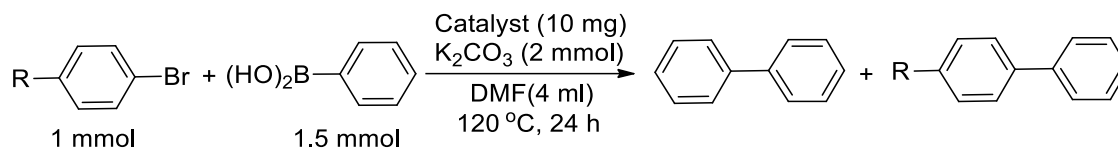
Table 2. Nitrogen sorption data at 273 K and 1 bar.

COFs	S_{BET} ($\text{m}^2 \text{g}^{-1}$)	S_{Lang} ($\text{m}^2 \text{g}^{-1}$)	Pore volume (cc g^{-1})
Pd(II)/TAT-DHBD (3)	139.0	331.1	0.143
Pd(II)/TAT-TFP (4)	292.0	388.0	0.145
Pd(0)/TAT-DHBD (5)	21.5	76.0	0.074
Pd(0)/TAT-TFP (6)	52.2	159.4	0.094

Catalytic studies

The catalytic activity of Pd(II)/TAT-DHBD (**3**), Pd(II)/TAT-TFP (**4**), Pd(0)/TAT-DHBD (**5**) and Pd(0)/TAT-TFP (**6**) has been examined for the carbon-carbon bond forming reactions through Suzuki-Miyaura coupling reaction. This reaction is mostly performed under homogeneous medium to achieve effective C-C bond formation.^[17a-b] However, the inability to recycle the catalyst has remained a major disadvantage when this reaction is carried out under homogeneous reaction conditions. To obviate this shortcoming, there have been reports in recent times where the catalyst has been embedded within solid matrices such MOFs and COFs.^{[5],[14]} Hence, the Pd incorporated COFs **3-6** have been utilized as active catalysts for C-C bond formation reactions in the present study.

The initially model reaction was performed with phenyl boronic acid (1.5 mmol) and bromobenzene (1 mmol) using K_2CO_3 (2 mmol) as a base and the COF catalyst (10 mg) in dimethylformamide (4 mL) at 100 °C for 24 h. The conversion of the reaction was monitored with the help of GC-MS and it was found that complete conversion was achieved within 24 h (Table 3). The catalytic activity of Pd-COFs was initially tested with unsubstituted bromobenzene, for which only moderate catalytic activity was observed. To check the selectivity in terms of homo/hetero coupling, substituted bromobenzenes were then employed. More than 80 % hetero-coupling products were identified in all the cases, revealing that the present catalysts are selective towards the desired heterocoupled products. The effect of substituents was also explored and it was established that the catalysts are more active when electron withdrawing substituent (-CN) was present on the aryl ring. Significantly, complete conversion (100 %) has been achieved within 4 h when 4-cyano bromobenzene was used (Table 3).

**Table 3:** Catalytic activity of Pd(0)/Pd(II)-COFs in Suzuki-Miyaura coupling reaction

Catalyst	R	Conversion (%)	Selectivity (%)	
			a	b
Pd(II)/TAT-DHBD (3)	H	56	-	-
	CH ₃	34	24	76
	OCH ₃	59	15	85
	CN	100	24	76
Pd(II)/TAT-TFP (4)	H	80	-	-
	CH ₃	60	25	75
	OCH ₃	67	19	81
	CN	100	-	100
Pd(0)/TAT-DHBD (5)	H	62	-	-
	CH ₃	49	20	80
	-OCH ₃	64	11	89
	-CN	100	3	97
Pd(0)/TAT-TFP (6)	-H	83	-	-
	-CH ₃	69	30	70
	-OCH ₃	73	16	84
	-CN	100	1	99

Reaction conditions: COF catalyst (10 mg), boronic acid (1.5 mmol), bromo compound (1 mmol), K₂CO₃ (2 mmol), dimethylformamide (4 ml), temperature (100 °C) and time (24 h).

These Pd-COFs have been investigated for their reusability for five successive (repeated) catalytic runs (Figure 12). To perform the reusability study, Pd(II)/TAT-TFP (4) and Pd(0)/TAT-TFP (6) catalysts have been chosen as they exhibit better catalytic activity compared to Pd(II)/TAT-DHBD (3) and Pd(0)/TAT-DHBD (5). Thus, at the end of each run the catalyst was repeatedly washed with water, ether and methanol and dried at 110 °C prior to every successive catalytic run. From this study, it emerges that these catalysts (4 and 6) are indeed reusable even after the fifth catalytic run (note that after the second run, the conversion more or less stabilizes to about 85-90%).

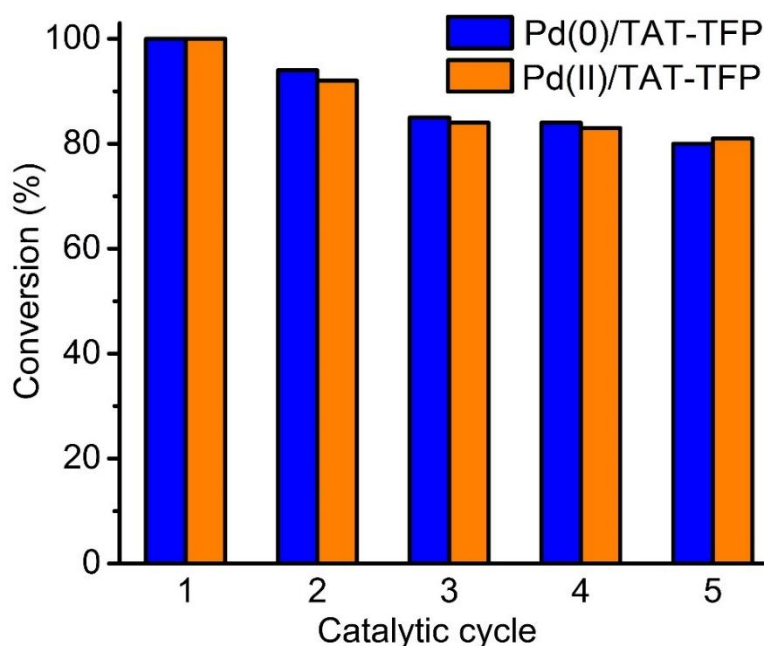


Figure 12: Reusability of Pd(II)/TAT-TFP (4) and Pd(0)/TAT-TFP (6) in C-C coupling reaction between phenyl boronic acid and 4-cyano bromo benzene.

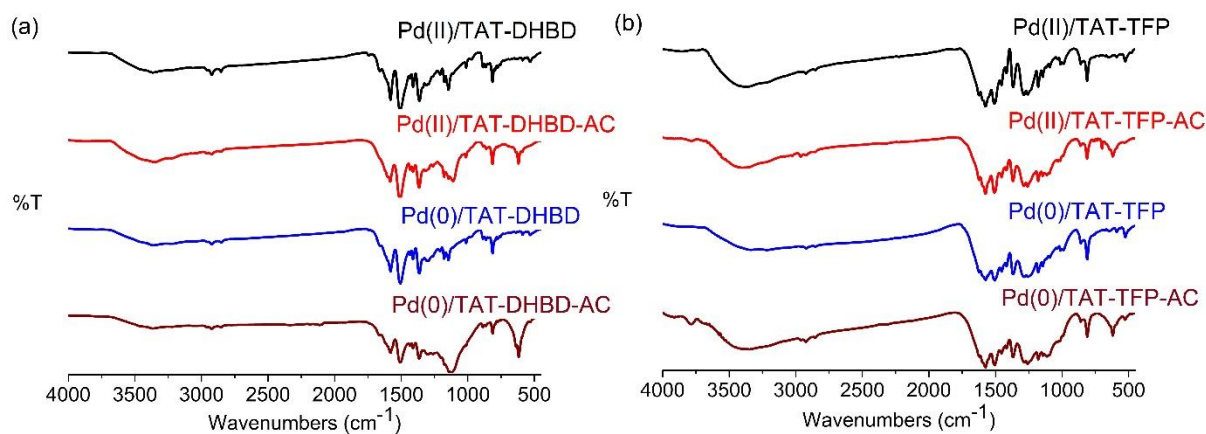


Figure 13. FT-IR spectra of Pd(II)/TAT-DHBD (3), Pd(II)/TAT-TFP (4), Pd(0)/TAT-DHBD (5) and Pd(0)/TAT-TFP (6) after the catalysis.

To evaluate the amount of palladium leaching after the third cycle, suitably washed and dried catalyst (Pd(II)/TAT-TFP (4) or Pd(0)/TAT-TFP (6)) was treated with K_2CO_3 in dimethylformamide at 100 °C for 4 h under constant stirring. The catalyst was then filtered and the solution collected was subjected to Inductively Coupled Plasma - Atomic Emission Spectroscopy (ICP-AES). These solutions exhibited no evidence for the presence of palladium species in the solution (< 0.25 ppm). This clearly confirms that there is no leaching of Pd(0)/Pd(II) from the catalysts that have been already subjected to three runs.

To further ascertain that these solutions contained no palladium, substrates 4-cyanoabromo benzene and phenylboronic acid were added to the above solution and stirred at 100 °C for 4 h, exhibiting no reaction. The IR spectra of the catalysts have also been compared before and after the catalytic reactions and found to be similar (Figure 13).

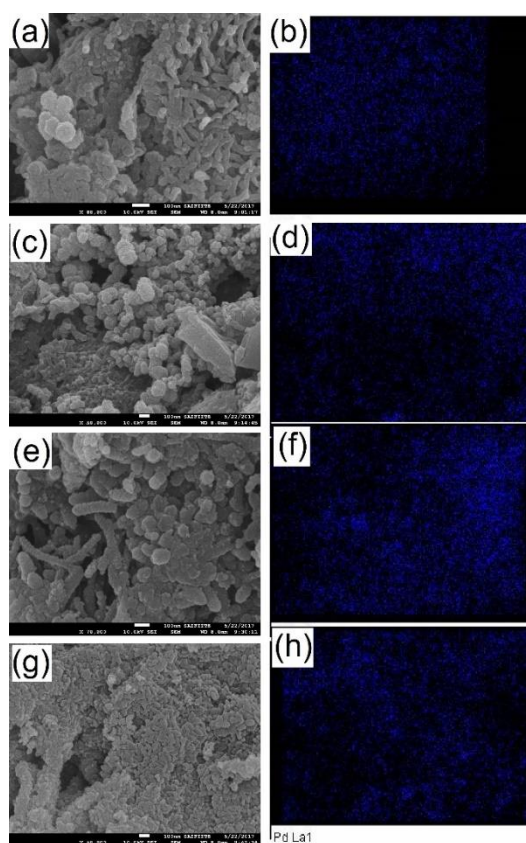


Figure 14. SEM images of Pd(II)/TAT-DHBD (3), Pd(II)/TAT-TFP (4), Pd(0)/TAT-DHBD (5) and Pd(0)/TAT-TFP (6) ((a), (c), (e), (g)) and their respective EDS for Pd ((b), (d), (f), (h)) after the catalysis

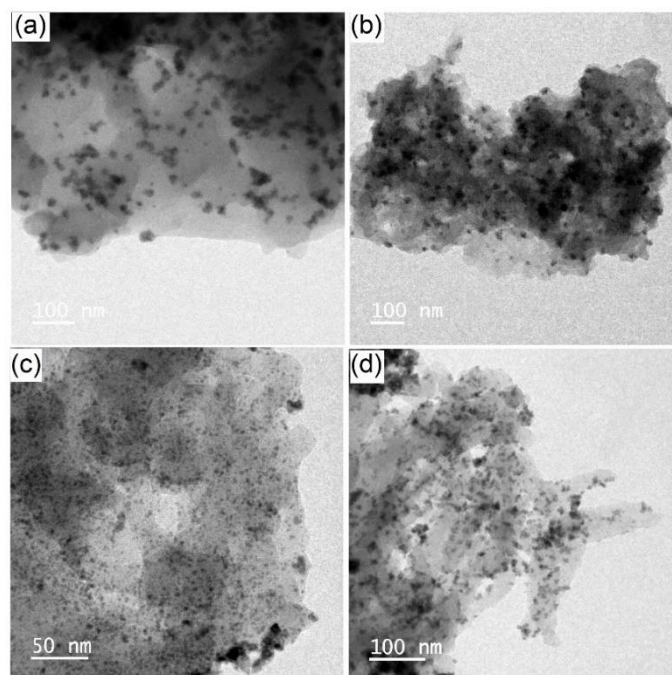


Figure 15. TEM images of (a) Pd(II)/TAT-DHBD (**3**), (b) Pd(II)/TAT-TFP (**4**), (c) Pd(0)/TAT-DHBD (**5**) and (d) Pd(0)/TAT-TFP (**6**) after three catalytic runs

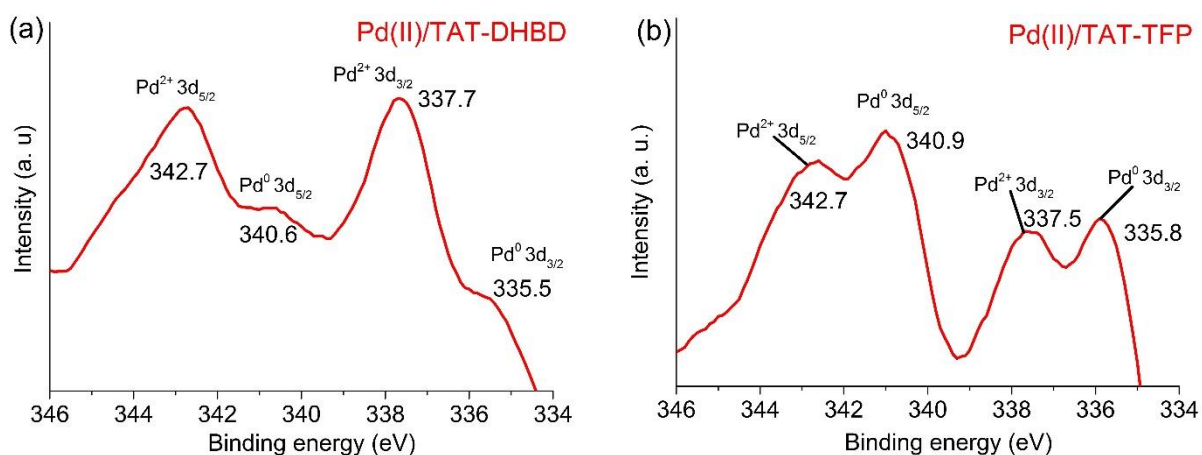


Figure 16. XPS spectra of (a) Pd(II)/TAT-DHBD (**3**) and (b) Pd(II)/TAT-TFP (**4**) in Pd 3d region after the catalysis.

The FE-SEM analysis shows that the morphology of the Pd loaded COFs remains unaltered after the catalytic runs. The EDX-elemental mapping analysis reveals that the Pd nanoparticles are well-dispersed on the COF material and not agglomerated after the reaction (Figure 14). This has further been confirmed by the TEM analysis. TEM images of the Pd incorporated COFs after the reaction shows homogeneously dispersed nano particles and the 2D sheets of COFs remain unaltered (Figure 15). In order to evaluate the oxidation state of Pd in **3** and **4** after three catalytic runs, XPS spectra have been recorded (Figure 16). The results obtained shows that the oxidation state of a small fraction of Pd centres is converted from +2

to 0 after catalysis, as has been previously reported for other Pd(II) incorporated polymeric materials.^[34]

CO₂ uptake studies

Nitrogen enriched pristine COFs and their Pd immobilized variants are expected to be CO₂-philic. Thus, these COFs has been utilized for the capture of CO₂. The Pd loaded polymers are mostly investigated for the hydrogen storage.^{[15],[35]} Barring a few,^[36] less attention has been given for CO₂ uptake. In order to evaluate the CO₂ uptake, the measurements were carried out at two different temperatures (273 and 298 K) and up to 1 bar (Figure 17). The results obtained are listed in Table 4. TAT-TFP (**2**) exhibited the highest CO₂ uptake of 17.1 wt% and 10.6 wt% at 273 and 298 K, respectively, at 1 bar, similar to a recent literature report.^[29a] In contrast, TAT-DHBD (**1**) showed low CO₂ uptake of 5.98 wt % and 3.5 wt % at 273 and 298 K, respectively, at 1 bar. Interestingly, even after immobilizing the Pd metal particles, Pd(II)/TAT-TFP (**4**) showed 11.0 and 7.5 wt % of CO₂ uptake while Pd(0)/TAT-TFP (**6**) exhibited 5.8 and 3.8 wt% of CO₂ uptake at 273 and 298 K, respectively. This CO₂ uptake is higher than that reported for Pd loaded polymer Azo-CPP-1-Pd (9.17 wt % at 273 K and 1 bar).^[35] It can be thus clearly established that Pd(II) is coordinated to only imine group and not to triazine functionality, which is still available for the CO₂ uptake. In case of Pd(0)/TAT-TFP (**6**), the nanoparticles are spread homogeneously all over the framework, masking the available nitrogen sites for interaction with CO₂. The CO₂ isotherms are completely reversible for all the COFs, which indicates that the interaction between CO₂ and the COFs is weak and the material can be easily regenerated without any external stimuli. The isosteric heats of adsorption (Q_{st}) calculated from Classius-Clayeperon equation is found to vary between 27.2 and 38.4 kJ mol⁻¹, as derived from the adsorption data collected at 273 and 298 K (Figure 18).

Table 4. CO₂ sorption data for TAT-DHBD (**1**), TAT-TFP (**2**), Pd(II)/TAT-DHBD (**3**), Pd(II)/TAT-TFP (**4**), Pd(0)/TAT-DHBD (**5**) and Pd(0)/TAT-TFP (**6**) at 1 bar.

COF	CO ₂ uptake at 273 K (wt%)	CO ₂ uptake at 298 K (wt%)	Q _{st} (kJ/mol)
TAT-DHBD (1)	5.98	3.46	27.24
TAT-TFP (2)	17.11	10.66	29.96
Pd(II)/TAT-DHBD (3)	4.55	3.20	38.40
Pd(II)/TAT-TFP (4)	11.01	7.50	29.96
Pd(0)/TAT-DHBD (5)	4.79	3.09	35.29
Pd(0)/TAT-TFP (6)	5.83	3.84	32.32

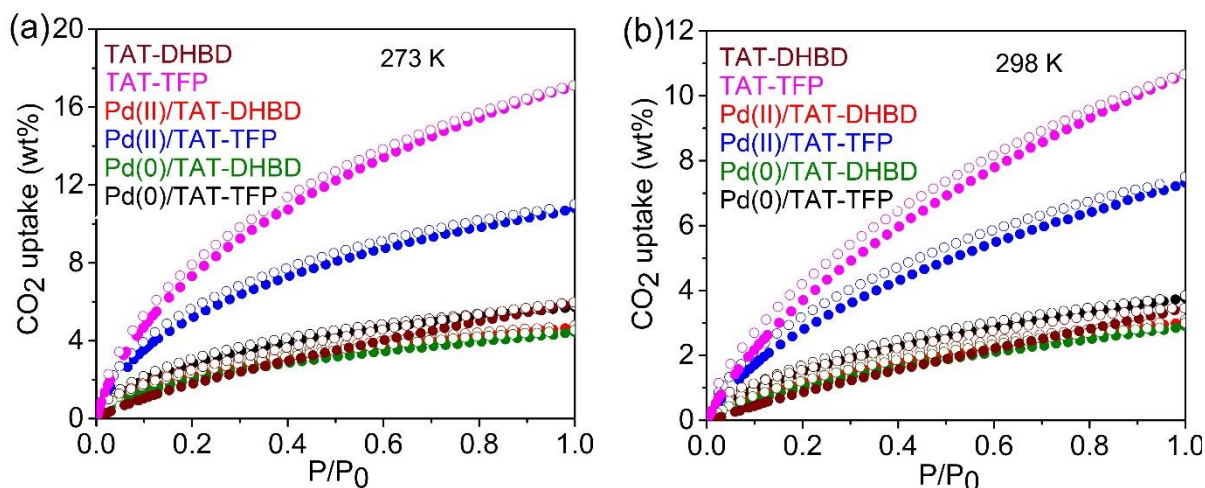


Figure 17. CO₂ adsorption isotherms at (a) 273 K and (b) 298 K for TAT-DHBD (1), TAT-TFP (2), Pd(II)/TAT-DHBD (3), Pd(II)/TAT-TFP (4), Pd(0)/TAT-DHBD (5) and Pd(0)/TAT-TFP (6) at 1 bar.

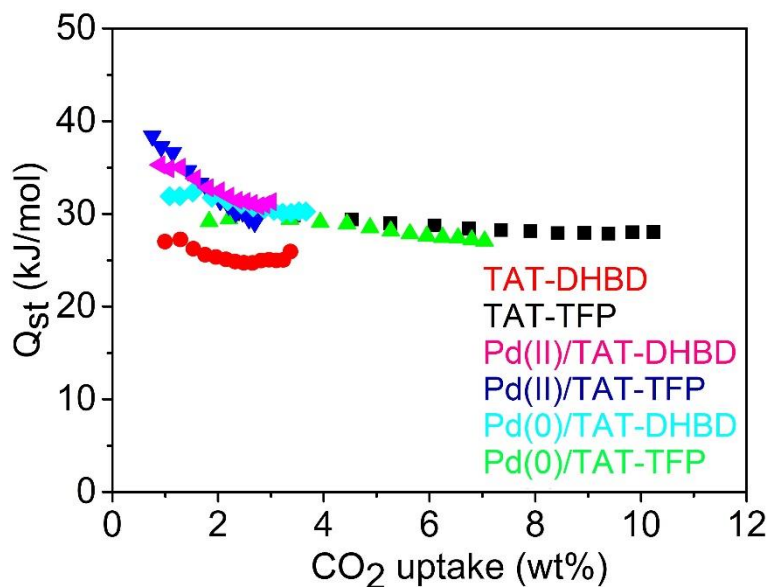


Figure 18. Isothermic heat of adsorption for TAT-DHBD (1), TAT-TFP (2), Pd(II)/TAT-DHBD (3), Pd(II)/TAT-TFP (4), Pd(0)/TAT-DHBD (5) and Pd(0)/TAT-TFP (6) at 1 bar.

Conclusions

Dihydroxybenzene-1,4-dicarboxaldehyde (DHBD) and triformylphloroglucinol (TFP) have been independently combined with tris(aminophenyl)triazine (TAT) to yield either imine or β -ketoenamine based mesoporous and microporous covalent organic frameworks, TAT-DHBD (1) and TAT-TFP (2), respectively, exhibiting high surface areas. The presence of abundant number of pyridinic and imine nitrogen centers in both these COFs apart from a number of

phenolic –OH groups, render them highly suitable for metal ion / metal nanoparticle incorporation. Choosing palladium as an example, it has been shown that these COFs are indeed excellent supports for Pd(II) complexes and Pd(0)-nanoparticles. These Pd loaded COFs are *useful heterogeneous catalysts* for the C-C bond forming Suzuki-Miyaura coupling reaction. It is particularly interesting to note that Pd(0)/TAT-TFP exhibits 100 % substrate conversion for the cross coupling of 4-cyano-bromobenzene within 4 hours. Besides, the utility of these Pd loaded COFs for CO₂ capture has also been explored.

It appears that the pristine frameworks **1** and **2** are very robust and can host other types of metal ions through N,O chelation (which has not been realized yet) with metal ions such as Mn, Co, Ru, etc. We are presently investigating these aspects with the objective of realizing newer heterogeneous catalysts for other organic transformation.

Experimental section

Methods, Materials and Instruments. See Supporting Information (S1)

Synthesis of TAT-Sal (7). 1,3,5-Tris(4'-aminophenyl)triazine (TAT) (0.050 g, 0.10 mmol) was dissolved in dry MeOH (20 mL). To this solution, a methanolic solution (in 5.0 mL) of salicylaldehyde (0.037 g, 0.035 mmol) and 2-3 drops of formic acid (cat.) were added. A precipitate started to appear upon heating the reaction mixture at reflux conditions for 30 minutes. The heating was continued for another 10 h. The crystalline product formed was collected by filtration and washed well with MeOH (30 mL x 3). Finally it was dried under vacuum to obtain off-white crystalline powder (0.04 g, 69 %) suitable for analysis. Mp.; 242 °C. Anal. Calcd for C₄₂H₃₀N₆O₃: C, 74.45 (75.66); H, 3.86 (4.54); N, 12.94 (12.60). ¹H NMR (400 MHz, CDCl₃): δ 13.1 (s, 3H, -OH), 8.86 (d, 6H, ArH), 8.73 (s, 3H, CH=N), 7.48 (d, 9H, ArH), 7.43 (t, 3H, ArH), 7.07 (d, 3H, ArH), 6.98 (t, 3H, ArH) ppm. ¹³C{¹H} NMR: δ 171.7, 163.9, 161.5, 152.4, 134.8, 133.9, 132.8, 130.6, 121.7, 119.5 and 117.6. FT-IR (KBr diluted disc); 3027, 2923, 2854, 1627(s), 1598, 1504, 1024, 829 cm⁻¹. ESI-MS calcd for C₄₅H₃₃N₃O₃⁺ [M]⁺ 666.23, found 667.54 [M+1]⁺.

Synthesis of TAT- DHBD (1). A mixture of 1,3,5-tris(4'-aminophenyl)triazine (TAT) (0.100 g, 0.28 mmol), DHBD (0.070 g, 0.42 mmol), 6 M aq. acetic acid (0.3 mL) and dry 1,4-dioxane (1.5 mL) and mesitylene (1.5 mL) was taken in a glass tube of dimension 10 × 8 mm (o.d. × i. d.). The mixture was sonicated for 10 mins to get a clear suspension. The tube was flash frozen at 77 K (liquid nitrogen bath) by three freeze-pump-thaw cycles and flame sealed under

vacuum. The sealed tube was heated at 120 °C for 3 days yielding orange precipitate. The precipitate was isolated by filtration and washed THF, acetone and dried under high vacuum for 7 h at 120 °C to afford TAT-DHBD. Yield - 0.070 g, (64 %). Anal. calcd for C₃₃H₂₁N₆O₃; found (Calcd): C, 58.07 (72.12); H, 3.47 (3.85); N, 13.79 (15.29). CP-MAS ¹³C{¹H} NMR (295 K): δ 160.7, 149.0, 146.0, 139.5, 137.1, 131.7, 128.1, 125.8, 121.3, 27.3, 22.5 ppm. FT-IR (KBr diluted disc); 3357, 2959, 2923, 2869, 1634, 1598, 1462, 1410, 1168 cm⁻¹.

Synthesis of TAT-TFP (2). This compound was prepared by following procedure described above. TAT (0.100 g, 0.28 mmol), 1,3,5-triformylphluoroglucinol (0.063 g, 0.28 mmol), 6 M aq. acetic acid (0.3 mL) and dry 1,4-dioxane (1.5 mL)/mesitylene (1.5 mL). Yield 0.060 g (43%). Anal. calcd for C₃₀H₁₉N₆O₃; found (calcd): C, 65.25 (70.44); H, 3.89 (3.74); N, 14.81 (16.43). CP-MAS ¹³C{¹H} NMR (295 K): δ 184.1, 146.4, 137.6, 137.2, 127.3, 120.3, 119.6, 115.5, 106.1 ppm. FT-IR (KBr diluted disc); 2924, 2852, 1619, 1593, 1574, 1455, 1293, 1262 cm⁻¹.

General procedure for Pd(II) incorporated COFs

The COFs **1** and **2** (100 mg) were dispersed in 50 mL of DCM in a 100 mL round bottomed flask. To this, Pd(OAc)₂ (30 mg) was added and stirred in room temperature for 24 hours. The Pd(II) incorporated COFs **3** and **5** were filtered, washed with DCM followed by acetone and dried in vacuum for 6 h at 120 °C.

Pd(II)/TAT-DHBD (3): Yield-0.115 g (93 %). Anal. calcd for C₇₈H₆₀N₁₂O₁₈Pd₃; found (calcd): C, 46.59 (52.85); H, 2.55 (3.41); N, 11.64 (9.48). CP-MAS ¹³C{¹H} NMR (295 K): δ 179.0, 167.8, 158.3, 150.7, 127.7, 120.1, 117.1, 114.7, 114.2 and 23.1 ppm. FT-IR (KBr diluted disc); 3366, 2923, 2852, 1740, 1662, 1579, 1505, 1411, 1362, 1176, 1144 and 814 cm⁻¹.

Pd(II)/TAT-TFP (4): Yield-0.120 g (95 %). Anal. calcd for C₇₂H₅₆N₁₂O₁₈Pd₃; found (calcd): C, 47.87 (50.97); H, 3.79 (3.33); N, 11.09 (9.91). CP-MAS ¹³C{¹H} NMR (295 K): δ 182.8, 182.1, 167.8, 145.7, 139.5, 128.6, 118.6, 112.5, 105.1 and 22.3 ppm. FT-IR (KBr diluted disc); 3368, 2922, 1623, 1574, 1508, 1454, 1367, 1286, 1257, 1179, 1145 and 811 cm⁻¹.

General procedure for Pd(0) incorporated COFs

The COFs **1** and **2** (100 mg) were dispersed in 50 mL of methanol in a 100 mL round bottomed flask. To this, Pd(OAc)₂ (30 mg) was added and stirred in room temperature for 1h.

Then NaBH₄ (100 mg) was added by small portion under 0 °C for 30 mins. The mixture was stirred in room temperature for 24 hours. The Pd(0) incorporated COFs were filtered, washed with copious amount of water followed by acetone and dried in vacuum for 6 h at 120 °C.

Pd(0)/TAT-DHBD (5): Yield-0.092 g (86 %). Anal. calcd for C₃₃H₂₁N₆O₃Pd; found (calcd): C, 54.14 (60.42); H, 3.69 (3.23); N, 13.24 (12.81). CP-MAS ¹³C{¹H} NMR (295 K): δ 167.8, 158.3, 150.7, 127.7, 120.1, 117.1, 114.7 and 114.2 ppm. FT-IR (KBr diluted disc); 3366, 2922, 2852, 1662, 1580, 1505, 1411, 1363, 1177, 1145 and 813 cm⁻¹.

Pd(0)/TAT-TFP (6): Yield-0.090 g (85 %). Anal. calcd for C₃₀H₁₉N₆O₃Pd; found (calcd): C, 52.15 (58.31); H, 4.09 (3.10); N, 11.98 (13.60). CP-MAS ¹³C{¹H} NMR (295 K): δ 184.0, 167.9, 145.9, 139.5, 128.7, 118.5, 112.0 and 104.9 ppm. FT-IR (KBr diluted disc); 3220, 2920, 1622, 1574, 1558, 1505, 1454, 1367, 1284, 1256, 1178 and 811 cm⁻¹.

Supporting Information

Methods, materials, instruments, ¹H and ¹³C NMR spectra of model compound, FT-IR spectra, TGA curves, PXRD, EDS mapping, HR-TEM and XPS spectra of all the COFs.

Acknowledgement

This work was supported by (1) SERB, New Delhi (SB/S1/IC-48/2013) and (2) IIT-Bombay Bridge Funding. R. M. thanks SERB, New Delhi for J. C. Bose Fellowship (SB/S2/JCB-85/2014). D. K. thanks UGC, New Delhi, and R. A. thanks SERB for NPDF fellowship (PDF/2017/00037). We thank the Pawsey supercomputing facility of CSIRO for the computing support.

Keywords: COFs, Palladium, Suzuki-Miyaura coupling, C-C bond formation, CO₂ uptake.

References

- [1] a) A. P. Cote, A. I. Benin, N. W. Ockwig, M. O'keeffe, A. J. Matzger, O. M. Yaghi, *science* **2005**, *310*, 1166-1170; b) S.-Y. Ding, W. Wang, *Chem. Soc. Rev.* **2013**, *42*, 548-568; c) X. Feng, X. Ding, D. Jiang, *Chem. Soc. Rev.* **2012**, *41*, 6010-6022; d) H. M. El-Kaderi, J. R. Hunt, J. L. Mendoza-Cortés, A. P. Côté, R. E. Taylor, M. O'keeffe, O. M. Yaghi, *Science* **2007**, *316*, 268-272; e) N. Huang, P. Wang, D. Jiang, *Nat. Rev. Mater.* **2016**, *1*, 16068; f) C. S. Diercks, O. M. Yaghi, *Science* **2017**, *355*, 923; g) N. Huang, L. Zhai, D. E. Coupry, M. A. Addicoat, K. Okushita, K. Nishimura, T. Heine,

- D. Jiang, *Nat. Commun.* **2016**, *7*, 12325; h) Z.-F. Pang, S.-Q. Xu, T.-Y. Zhou, R.-R. Liang, T.-G. Zhan, X. Zhao, *J. Am. Chem. Soc.* **2016**, *138*, 4710-4713; i) B. J. Smith, L. R. Parent, A. C. Overholts, P. A. Beaucage, R. P. Bisbey, A. D. Chavez, N. Hwang, C. Park, A. M. Evans, N. C. Gianneschi, *ACS Cent. Sci.* **2017**, *3*, 58-65.
- [2] a) X. Chen, M. Addicoat, E. Jin, L. Zhai, H. Xu, N. Huang, Z. Guo, L. Liu, S. Irle, D. Jiang, *J. Am. Chem. Soc.* **2015**, *137*, 3241-3247; b) J. L. Segura, M. J. Mancheño, F. Zamora, *Chem. Soc. Rev.* **2016**, *45*, 5635-5671.
- [3] a) S. S. Han, H. Furukawa, O. M. Yaghi, W. A. Goddard Iii, *J. Am. Chem. Soc.* **2008**, *130*, 11580-11581; b) H. Furukawa, O. M. Yaghi, *J. Am. Chem. Soc.* **2009**, *131*, 8875-8883; c) R. Ge, D. Hao, Q. Shi, B. Dong, W. Leng, C. Wang, Y. Gao, *J. Chem. Eng. Data* **2016**, *61*, 1904-1909; d) C. J. Doonan, D. J. Tranchemontagne, T. G. Glover, J. R. Hunt, O. M. Yaghi, *Nat. Chem.* **2010**, *2*, 235-238. d) N. Huang, X. Chen, R. Krishna, D. Jiang, *Angew. Chem. Int. Ed.* **2015**, *54*, 2986-2990; e) Y. Zeng, R. Zou, Y. Zhao, *Adv. Mater.* **2016**, *28*, 2855-2873; f) Z. Li, Y. Zhi, X. Feng, X. Ding, Y. Zou, X. Liu, Y. Mu, *Chem. Eur. J.* **2015**, *21*, 12079-12084; g) N. Huang, R. Krishna, D. Jiang, *J. Am. Chem. Soc.* **2015**, *137*, 7079-7082; i) H. Lu, C. Wang, J. Chen, R. Ge, W. Leng, B. Dong, J. Huang, Y. Gao, *Chem. Commun.* **2015**, *51*, 15562-15565; j) J. Fu, S. Das, G. Xing, T. Ben, V. Valtchev, S. Qiu, *J. Am. Chem. Soc.* **2016**, *138*, 7673-7680; k) H.-L. Qian, C.-X. Yang, X.-P. Yan, *Nat. Commun.* **2016**, *7*, 12104; l) S. Zhao, B. Dong, R. Ge, C. Wang, X. Song, W. Ma, Y. Wang, C. Hao, X. Guo, Y. Gao, *RSC Adv.* **2016**, *6*, 38774-38781; m) L. Stegbauer, M. W. Hahn, A. Jentys, G. k. Savasci, C. Ochsenfeld, J. A. Lercher, B. V. Lotsch, *Chem. Mater.* **2015**, *27*, 7874-7881.
- [4] a) H. Zhao, Z. Jin, H. Su, X. Jing, F. Sun, G. Zhu, *Chem. Commun.* **2011**, *47*, 6389-6391; b) Q. Fang, J. Wang, S. Gu, R. B. Kaspar, Z. Zhuang, J. Zheng, H. Guo, S. Qiu, Y. Yan, *J. Am. Chem. Soc.* **2015**, *137*, 8352-8355; c) L. Bai, S. Z. F. Phua, W. Q. Lim, A. Jana, Z. Luo, H. P. Tham, L. Zhao, Q. Gao, Y. Zhao, *Chem. Commun.* **2016**, *52*, 4128-4131.
- [5] a) H. Xu, J. Gao, D. Jiang, *Nat. Chem.* **2015**, *7*, 905-912; b) S. Lin, C. S. Diercks, Y.-B. Zhang, N. Kornienko, E. M. Nichols, Y. Zhao, A. R. Paris, D. Kim, P. Yang, O. M. Yaghi, *Science* **2015**, *349*, 1208-1213; c) Q. Fang, S. Gu, J. Zheng, Z. Zhuang, S. Qiu, Y. Yan, *Angew. Chem. Int. Ed.* **2014**, *53*, 2878-2882; d) V. S. Vyas, F. Haase, L. Stegbauer, G. Savasci, F. Podjaski, C. Ochsenfeld, B. V. Lotsch, *Nat. Commun.* **2015**, *6*, 8508; e) X. Wang, X. Han, J. Zhang, X. Wu, Y. Liu, Y. Cui, *J. Am. Chem. Soc.* **2016**, *138*, 12332-12335; f) S.-Y. Ding, J. Gao, Q. Wang, Y. Zhang, W.-G. Song, C.-Y. Su,

- W. Wang, *J. Am. Chem. Soc.* **2011**, *133*, 19816-19822; g) D. B. Shinde, S. Kandambeth, P. Pachfule, R. R. Kumar, R. Banerjee, *Chem. Commun.* **2015**, *51*, 310-313; h) P. Pachfule, S. Kandambeth, D. D. Díaz, R. Banerjee, *Chem. Commun.* **2014**, *50*, 3169-3172; i) P. Pachfule, M. K. Panda, S. Kandambeth, S. Shivaprasad, D. D. Díaz, R. Banerjee, *J. Mater. Chem. A* **2014**, *2*, 7944-7952; j) J. Thote, H. B. Aiyappa, A. Deshpande, D. Díaz Díaz, S. Kurungot, R. Banerjee, *Chem. Eur. J.* **2014**, *20*, 15961-15965; k) M. Bhadra, H. S. Sasmal, A. Basu, S. P. Midya, S. Kandambeth, P. Pachfule, E. Balaraman, R. Banerjee, *ACS Appl. Mater. Interfaces* **2017**, *9*, 13785-13792.
- [6] a) M. Calik, F. Auras, L. M. Salonen, K. Bader, I. Grill, M. Handloser, D. D. Medina, M. Dogru, F. Löbermann, D. Trauner, *J. Am. Chem. Soc.* **2014**, *136*, 17802-17807; b) F. Xu, S. Jin, H. Zhong, D. Wu, X. Yang, X. Chen, H. Wei, R. Fu, D. Jiang, *Sci. Rep.* **2015**, *5*, 8225; c) C. R. DeBlase, K. E. Silberstein, T.-T. Truong, H. D. Abruña, W. R. Dichtel, *J. Am. Chem. Soc.* **2013**, *135*, 16821-16824; d) F. Xu, H. Xu, X. Chen, D. Wu, Y. Wu, H. Liu, C. Gu, R. Fu, D. Jiang, *Angew. Chem. Int. Ed.* **2015**, *54*, 6814-6818; e) C. R. DeBlase, K. Hernandez-Burgos, K. E. Silberstein, G. G. Rodríguez-Calero, R. P. Bisbey, H. D. Abruña, W. R. Dichtel, *ACS Nano* **2015**, *9*, 3178-3183; f) H. Liao, H. Wang, H. Ding, X. Meng, H. Xu, B. Wang, X. Ai, C. Wang, *J. Mater. Chem. A* **2016**, *4*, 7416-7421; g) A. M. Khattak, Z. A. Ghazi, B. Liang, N. A. Khan, A. Iqbal, L. Li, Z. Tang, *J. Mater. Chem. A* **2016**, *4*, 16312-16317.
- [7] a) S.-Y. Ding, M. Dong, Y.-W. Wang, Y.-T. Chen, H.-Z. Wang, C.-Y. Su, W. Wang, *J. Am. Chem. Soc.* **2016**, *138*, 3031-3037; b) Q. Sun, B. Aguila, J. Perman, L. D. Earl, C. W. Abney, Y. Cheng, H. Wei, N. Nguyen, L. Wojtas, S. Ma, *J. Am. Chem. Soc.* **2017**, *139*, 2786-2793; c) N. Huang, L. Zhai, H. Xu, D. Jiang, *J. Am. Chem. Soc.* **2017**, *139*, 2428-2434.
- [8] a) S. Kandambeth, B. P. Biswal, H. D. Chaudhari, K. C. Rout, H. Kunjattu, S. Mitra, S. Karak, A. Das, R. Mukherjee, U. K. Kharul, *Adv. Mater.* **2017**, *29*, 1603945; b) J. Dong, Y. Wang, G. Liu, Y. Cheng, D. Zhao, *CrystEngComm* **2017**, *19*, 4899-4904 ; c) Y. Ying, W. Ying, Q. Li, D. Meng, G. Ren, R. Yan, X. Peng, *Appl. Mater. Today* **2017**, *7*, 144-158.
- [9] a) S. Chandra, T. Kundu, S. Kandambeth, R. BabaRao, Y. Marathe, S. M. Kunjir, R. Banerjee, *J. Am. Chem. Soc.* **2014**, *136*, 6570-6573; b) S. Chandra, T. Kundu, K. Dey, M. Addicoat, T. Heine, R. Banerjee, *Chem. Mater.* **2016**, *28*, 1489-1494; c) H. Xu, S. Tao, D. Jiang, *Nat. Mater.* **2016**, *15*, 722-726; d) H. Ma, B. Liu, B. Li, L. Zhang, Y.-G. Li, H.-Q. Tan, H.-Y. Zang, G. Zhu, *J. Am. Chem. Soc.* **2016**, *138*, 5897-5903; e) Y.

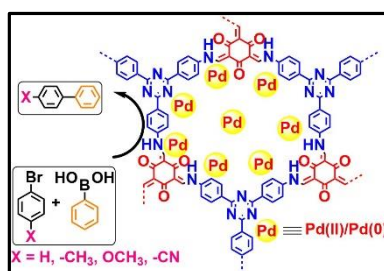
- Peng, G. Xu, Z. Hu, Y. Cheng, C. Chi, D. Yuan, H. Cheng, D. Zhao, *ACS Appl. Mater. Interfaces* **2016**, *8*, 18505-18512.
- [10] a) S. Dalapati, S. Jin, J. Gao, Y. Xu, A. Nagai, D. Jiang, *J. Am. Chem. Soc.* **2013**, *135*, 17310-17313; b) D. Kaleeswaran, P. Vishnoi, R. Murugavel, *J. Mater. Chem. C* **2015**, *3*, 7159-7171; c) G. Das, B. P. Biswal, S. Kandambeth, V. Venkatesh, G. Kaur, M. Addicoat, T. Heine, S. Verma, R. Banerjee, *Chem. Sci.* **2015**, *6*, 3931-3939; d) Y. Zhang, A. Sigen, Y. Zou, X. Luo, Z. Li, H. Xia, X. Liu, Y. Mu, *J. Mater. Chem. A* **2014**, *2*, 13422-13430; e) S. Wan, J. Guo, J. Kim, H. Ihee, D. Jiang, *Angew. Chem. Int. Ed.* **2009**, *48*, 5439-5442; f) S. Dalapati, E. Jin, M. Addicoat, T. Heine, D. Jiang, *J. Am. Chem. Soc.* **2016**, *138*, 5797-5800; g) G. Lin, H. Ding, D. Yuan, B. Wang, C. Wang, *J. Am. Chem. Soc.* **2016**, *138*, 3302-3305.
- [11] a) N. Huang, X. Ding, J. Kim, H. Ihee, D. Jiang, *Angew. Chem.* **2015**, *127*, 8828-8831; b) J. W. Crowe, L. A. Baldwin, P. L. McGrier, *J. Am. Chem. Soc.* **2016**, *138*, 10120-10123; c) S. Wan, J. Guo, J. Kim, H. Ihee, D. Jiang, *Angew. Chem.* **2008**, *120*, 8958-8962; d) H. Ding, Y. Li, H. Hu, Y. Sun, J. Wang, C. Wang, C. Wang, G. Zhang, B. Wang, W. Xu, *Chem. Eur. J.* **2014**, *20*, 14614-14618; e) L. Chen, K. Furukawa, J. Gao, A. Nagai, T. Nakamura, Y. Dong, D. Jiang, *J. Am. Chem. Soc.* **2014**, *136*, 9806-9809; f) Y. Du, D. Calabro, B. Wooler, P. Kortunov, Q. Li, S. Cundy, K. Mao, *Chem. Mater.* **2015**, *27*, 1445-1447; g) G. H. Bertrand, V. K. Michaelis, T.-C. Ong, R. G. Griffin, M. Dincă, *Proc. Natl. Acad. Sci. USA* **2013**, *110*, 4923-4928.
- [12] a) J. Guo, Y. Xu, S. Jin, L. Chen, T. Kaji, Y. Honsho, M. A. Addicoat, J. Kim, A. Saeki, H. Ihee, *Nat. Commun.* **2013**, *4*, 2736; b) X. Ding, L. Chen, Y. Honsho, X. Feng, O. Saengsawang, J. Guo, A. Saeki, S. Seki, S. Irle, S. Nagase, *J. Am. Chem. Soc.* **2011**, *133*, 14510-14513; c) S. Jin, X. Ding, X. Feng, M. Supur, K. Furukawa, S. Takahashi, M. Addicoat, M. E. El-Khouly, T. Nakamura, S. Irle, *Angew. Chem. Int. Ed.* **2013**, *52*, 2017-2021.
- [13] a) R. Palkovits, M. Antonietti, P. Kuhn, A. Thomas, F. Schüth, *Angew. Chem. Int. Ed.* **2009**, *48*, 6909-6912; b) C. E. Chan-Thaw, A. Villa, L. Prati, A. Thomas, *Chem. Eur. J.* **2011**, *17*, 1052-1057; c) C. E. Chan-Thaw, A. Villa, P. Katekomol, D. Su, A. Thomas, L. Prati, *Nano Lett.* **2010**, *10*, 537-541; d) S. B. Kalidindi, K. Yusenko, R. A. Fischer, *Chem. Commun.* **2011**, *47*, 8506-8508; e) W. Leng, Y. Peng, J. Zhang, H. Lu, X. Feng, R. Ge, B. Dong, B. Wang, X. Hu, Y. Gao, *Chem. Eur. J.* **2016**, *22*, 9087-9091; f) C. A. Wang, Y. W. Li, X. M. Hou, Y. F. Han, K. Nie, J. P. Zhang, *ChemistrySelect* **2016**, *1*, 1371-1376; g) C. Xu, S. Afewerki, C. W. Tai, A. Córdova, N. Hedin, *ChemistrySelect*

- 2016**, *1*, 5801-5804; h) P. Zhang, Z. Weng, J. Guo, C. Wang, *Chem. Mater.* **2011**, *23*, 5243-5249; i) H. Zhong, C. Liu, H. Zhou, Y. Wang, R. Wang, *Chem. Eur. J.* **2016**, *22*, 12533-12541; j) Y. Zhou, Z. Xiang, D. Cao, C.-J. Liu, *Chem. Commun.* **2013**, *49*, 5633-5635; k) D. Mullangi, S. Nandi, S. Shalini, S. Sreedhala, C. P. Vinod, R. Vaidhyathan, *Sci. Rep.* **2015**, *5*, 10876.
- [14] a) A. Corma, H. García, F. Llabrés i Xamena, *Chem. Rev.* **2010**, *110*, 4606-4655; b) Y. K. Hwang, D. Y. Hong, J. S. Chang, S. H. Jung, Y. K. Seo, J. Kim, A. Vimont, M. Daturi, C. Serre, G. Férey, *Angew. Chem. Int. Ed.* **2008**, *47*, 4144-4148; c) J. Lee, O. K. Farha, J. Roberts, K. A. Scheidt, S. T. Nguyen, J. T. Hupp, *Chem. Soc. Rev.* **2009**, *38*, 1450-1459; d) J. Long, H. Liu, S. Wu, S. Liao, Y. Li, *ACS Catal.* **2013**, *3*, 647-654; e) M. Yadav, Q. Xu, *Chem. Commun.* **2013**, *49*, 3327-3329; f) X.-L. Yang, M.-H. Xie, C. Zou, Y. He, B. Chen, M. O'Keeffe, C.-D. Wu, *J. Am. Chem. Soc.* **2012**, *134*, 10638-10645; g) L. Zhu, X.-Q. Liu, H.-L. Jiang, L.-B. Sun, *Chem. Rev.* **2017**, *117*, 8129-8176.
- [15] S. B. Kalidindi, H. Oh, M. Hirscher, D. Esken, C. Wiktor, S. Turner, G. Van Tendeloo, R. A. Fischer, *Chem. Eur. J.* **2012**, *18*, 10848-10856.
- [16] a) B. Akermark, L. Ebersson, E. Jonsson, E. Pettersson, *J. Org. Chem.* **1975**, *40*, 1365-1367; b) N. T. Phan, M. Van Der Sluys, C. W. Jones, *Adv. Synth. Catal.* **2006**, *348*, 609-679; c) W. Niu, L. Zhang, G. Xu, *Acs Nano* **2010**, *4*, 1987-1996.
- [17] a) N. Miyaura, A. Suzuki, *Chem. Rev.* **1995**, *95*, 2457-2483; b) D. J. Cárdenas, *Angew. Chem. Int. Ed.* **1999**, *38*, 3018-3020; c) X. Chen, K. M. Engle, D. H. Wang, J. Q. Yu, *Angew. Chem. Int. Ed.* **2009**, *48*, 5094-5115; d) K. Sonogashira, *J. Organomet. Chem.* **2002**, *653*, 46-49; e) M. T. Reetz, E. Westermann, *Angew. Chem. Int. Ed.* **2000**, *39*, 165-168.
- [18] S. Kandambeth, A. Mallick, B. Lukose, M. V. Mane, T. Heine, R. Banerjee, *J. Am. Chem. Soc.* **2012**, *134*, 19524-19527.
- [19] a) S. Ren, M. J. Bojdys, R. Dawson, A. Laybourn, Y. Z. Khimiyak, D. J. Adams, A. I. Cooper, *Adv. Mater.* **2012**, *24*, 2357-2361; b) A. Modak, M. Pramanik, S. Inagaki, A. Bhaumik, *J. Mater. Chem. A* **2014**, *2*, 11642-11650; c) M. K. Bhunia, S. K. Das, P. Pachfule, R. Banerjee, A. Bhaumik, *Dalton Trans.* **2012**, *41*, 1304-1311; d) A. Bhunia, V. Vasylyeva, C. Janiak, *Chem. Commun.* **2013**, *49*, 3961-3963.
- [20] a) B. Ashourirad, A. K. Sekizkardes, S. Altarawneh, H. M. El-Kaderi, *Chem. Mater.* **2015**, *27*, 1349-1358; b) K. V. Rao, R. Haldar, T. K. Maji, S. J. George, *Polymer* **2014**, *55*, 1452-1458; c) D. M. D'Alessandro, B. Smit, J. R. Long, *Angew. Chem. Int. Ed.* **2010**, *49*, 6058-6082; d) N. MacDowell, N. Florin, A. Buchard, J. Hallett, A. Galindo,

- G. Jackson, C. S. Adjiman, C. K. Williams, N. Shah, P. Fennell, *Energy Environ. Sci.* **2010**, *3*, 1645-1669.
- [21] H. A. Patel, S. H. Je, J. Park, D. P. Chen, Y. Jung, C. T. Yavuz, A. Coskun, *Nat. Commun.* **2013**, *4*, 1357.
- [22] a) G. T. Rochelle, *Science* **2009**, *325*, 1652-1654; b) R. S. Haszeldine, *Science* **2009**, *325*, 1647-1652.
- [23] A. B. Rao, E. S. Rubin, *Environ. Sci. Technol.* **2002**, *36*, 4467-4475.
- [24] S. Choi, J. H. Drese, C. W. Jones, *ChemSusChem* **2009**, *2*, 796-854.
- [25] W. Shen, W. Fan, *J. Mater. Chem. A* **2013**, *1*, 999-1013.
- [26] a) J. Liu, P. K. Thallapally, B. P. McGrail, D. R. Brown, J. Liu, *Chem. Soc. Rev.* **2012**, *41*, 2308-2322; b) S. D. Kenarsari, D. Yang, G. Jiang, S. Zhang, J. Wang, A. G. Russell, Q. Wei, M. Fan, *RSC Adv.* **2013**, *3*, 22739-22773; c) K. Sumida, D. L. Rogow, J. A. Mason, T. M. McDonald, E. D. Bloch, Z. R. Herm, T.-H. Bae, J. R. Long, *Chem. Rev.* **2011**, *112*, 724-781.
- [27] a) D. Yuan, W. Lu, D. Zhao, H. C. Zhou, *Adv. Mater.* **2011**, *23*, 3723-3725; b) W. Lu, J. P. Sculley, D. Yuan, R. Krishna, Z. Wei, H. C. Zhou, *Angew. Chem. Int. Ed.* **2012**, *51*, 7480-7484; c) W. Lu, D. Yuan, J. Sculley, D. Zhao, R. Krishna, H.-C. Zhou, *J. Am. Chem. Soc.* **2011**, *133*, 18126-18129; d) T. Ben, H. Ren, S. Ma, D. Cao, J. Lan, X. Jing, W. Wang, J. Xu, F. Deng, J. M. Simmons, *Angew. Chem.* **2009**, *121*, 9621-9624; e) Y. Luo, B. Li, W. Wang, K. Wu, B. Tan, *Adv. Mater.* **2012**, *24*, 5703-5707; f) R. Swaidan, B. Ghanem, E. Litwiller, I. Pinnau, *Macromolecules* **2015**, *48*, 6553-6561; g) S. K. Gupta, D. Kaleeswaran, S. Nandi, R. Vaidhyanathan, R. Murugavel, *ACS Omega* **2017**, *2*, 3572-3582.
- [28] a) F. J. Uribe-Romo, J. R. Hunt, H. Furukawa, C. Klöck, M. O'Keeffe, O. M. Yaghi, *J. Am. Chem. Soc.* **2009**, *131*, 4570-4571; b) P. Pandey, A. P. Katsoulidis, I. Eryazici, Y. Wu, M. G. Kanatzidis, S. T. Nguyen, *Chem. Mater.* **2010**, *22*, 4974-4979.
- [29] a) R. Gomes, A. Bhaumik, *RSC Adv.* **2016**, *6*, 28047-28054; b) S. Karak, S. Kandambeth, B. P. Biswal, H. S. Sasmal, S. Kumar, P. Pachfule, R. Banerjee, *J. Am. Chem. Soc.* **2017**, *139*, 1856-1862.
- [30] *Material Studio Modeling Environment*, Release 7; Accelrys Software Inc.: San Diego, CA, USA, 2014.
- [31] a) W. Zhou, H. Wu, T. Yildirim, *Chem. Phys. Lett.* **2010**, *499*, 103-107; b) B. Lukose, A. Kuc, T. Heine, *Chem. Eur. J.* **2011**, *17*, 2388-2392; c) E. L. Spitler, B. T. Koo, J. L. Novotney, J. W. Colson, F. J. Uribe-Romo, G. D. Gutierrez, P. Clancy, W. R. Dichtel,

- J. Am. Chem. Soc.* **2011**, *133*, 19416-19421; d) B. T. Koo, W. R. Dichtel, P. Clancy, *J. Mater. Chem.* **2012**, *22*, 17460-17469; e) Q. Fang, Z. Zhuang, S. Gu, R. B. Kaspar, J. Zheng, J. Wang, S. Qiu, Y. Yan, *Nat. Commun.* **2014**, *5*, 4503; f) J. Gao, D. Jiang, *Chem. Commun.* **2016**, *52*, 1498-1500.
- [32] Y. Zhang, Y. Zhu, J. Guo, S. Gu, Y. Wang, Y. Fu, D. Chen, Y. Lin, G. Yu, C. Pan, *Phys. Chem. Chem. Phys.* **2016**, *18*, 11323-11329.
- [33] Poor solubility of all the COFs even in strong acids precluded the elemental analysis by ICP-AES studies in solution
- [34] a) J. Chen, J. Zhang, D. Zhu, T. Li, *J. Porous Mater.* **2016**, 847-853; b) R. S. Gonçalves, A. B. de Oliveira, H. C. Sindra, B. S. Archanjo, M. E. Mendoza, L. S. Carneiro, C. D. Buarque, P. M. Esteves, *ChemCatChem* **2016**, *8*, 743-750.
- [35] S. B. Kalidindi, R. A. Fischer, *Phys. Status Solidi B* **2013**, *250*, 1119-1127.
- [36] L. Tao, F. Niu, D. Zhang, J. Liu, T. Wang, Q. Wang, *RSC Adv.* **2015**, *5*, 96871-96878.

TOC and Synopsis



Pd(II) and Pd(0) incorporated meso and microporous imine and β -ketoenamine linked covalent organic frameworks exhibiting significant catalytic activity towards C-C cross coupling reaction and CO_2 capture